

# Evaluation of North Eurasian snow-off dates in the ECHAM5.4 atmospheric GCM

**P. Räisänen<sup>1</sup>, A. Luomaranta<sup>1</sup>, H. Järvinen<sup>2</sup>, M. Takala<sup>1</sup>, K. Jylhä<sup>1</sup>, O. N. Bulygina<sup>3</sup>,  
K. Luojus<sup>1</sup>, A. Riihelä<sup>1</sup>, A. Laaksonen<sup>1,4</sup>, J. Koskinen<sup>5</sup>, and J. Pulliainen<sup>1</sup>**

<sup>1</sup>Finnish Meteorological Institute, Helsinki, Finland

<sup>2</sup>Department of Physics, University of Helsinki, Helsinki, Finland

<sup>3</sup>All-Russian Research Institute of Hydrometeorological Information,  
World Data Centre, Obninsk, Russian Federation (RIHMI-WDC), Russia

<sup>4</sup>Department of Physics, University of Eastern Finland, Kuopio, Finland

<sup>5</sup>Finnish Geodetic Institute, Masala, Finland

Correspondence to: P. Räisänen (petri.raisanen@fmi.fi)

## Abstract

The timing of springtime end of snow melt (snow-off date) in Northern Eurasia in version 5.4 of the ECHAM5 atmospheric GCM is evaluated through comparison with a snow-off date dataset based on space-borne microwave radiometer measurements and with Russian snow course data. ECHAM5 reproduces well the observed gross geographical pattern of snow-off dates, with earliest snow-off (in March) in the Baltic region and latest snow-off (in June) in the Taymyr Peninsula and in northeastern parts of the Russian Far East. The primary biases are (1) a delayed snow-off in southeastern Siberia (associated with too low springtime temperature and too high surface albedo, in part due to insufficient shielding by canopy); and (2) an early bias in the western and northern parts of Northern Eurasia. Several sensitivity experiments were conducted, where biases in simulated atmospheric circulation were corrected through nudging and/or the treatment of surface albedo was modified. While this alleviated some of the model biases in snow-off dates, 2 m temperature and surface albedo, especially the early bias in snow-off in the western parts of Northern Eurasia proved very robust and was actually larger in the nudged runs.

A key issue underlying the snow-off biases in ECHAM5 is that snow melt occurs at too low temperatures. Very likely, this is related to the treatment of the surface energy budget. On one hand, the surface temperature  $T_s$  is not computed separately for the snow-covered and snow-free parts of the grid cells, which prevents  $T_s$  from rising above  $0^\circ\text{C}$  before all snow has vanished. Consequently, too much of the surface net radiation is consumed in melting snow and too little in heating the air. On the other hand, ECHAM5 does not include a canopy layer. Thus, while the albedo reduction due to canopy is accounted for, the shielding of snow on ground by the overlying canopy is not considered, which leaves too much solar radiation available for melting snow.

## 25 1 Introduction

25 Snow cover is one of the most important elements in the climate and hydrology of the Northern Hemisphere. Large areas of the Eurasian and North American continents are covered by seasonal snow. The varying snow cover affects directly the surface energy balance by interfering with the energy storage, net radiation and fluxes of sensible and latent  
30 heat. A significant positive feedback mechanism of the snow, albedo and solar radiation amplifies the climatic effects related to the snow cover: decreasing snow cover reduces the surface albedo and increases the amount of absorbed solar radiation at the surface, leading to increased melting and further reduction in the snow cover. The snow-albedo feedback is largest when changes in snow cover area are linked with substantial changes  
35 in regional albedo (Brown, 2000). This coincides with the maximum influence of snow cover on surface net radiation in spring, typically in April and May, when strong solar radiation and snow cover co-exist (Groisman et al., 1994). Snow cover also serves as a fresh water reservoir, thus regulating run-off in winter and spring, and influencing soil moisture content. Typically, delayed snow melt can increase spring and summer soil moisture content  
40 which can further contribute to cooler and wetter weather conditions even after the snow melt (Cohen, 1994), and conversely for early snow melt (Wetherald and Manabe, 1995; Rowell and Jones, 2006; Kendon et al., 2010).

The key climatic role of snow cover has prompted a wide range of observational and modelling studies on the topic. These include several intercomparisons of snow conditions simulated by atmospheric and fully coupled general circulation models (GCMs)  
45 with observational data (Foster et al., 1996; Frei and Robinson, 1998; Frei et al., 2003, 2005; Roesch, 2006; Derksen and Brown, 2012; Brutel-Vuilmet et al., 2013). Most recently, Brutel-Vuilmet et al. (2013) evaluated the snow cover simulated by models participating in Phase 5 of the Coupled Model Intercomparison Project (CMIP5). In terms of the multi-model  
50 average, the models reproduced the observed snow cover extent very well, with a slight tendency toward too late snow melt in Eurasia and too early snow melt in northern North America. However, there was still substantial inter-model dispersion around the multi-model

average. Moreover, the results highlighted two issues already found in earlier intercomparison studies. First, the interannual variability in Northern Hemisphere snow cover extent  
55 was underestimated by almost all models, which was already noted by Frei and Robinson (1998) in an analysis of Atmospheric Model Intercomparison Project, phase 1 (AMIP1) models. Second, the models underestimated considerably the observed negative trend in snow cover in spring (for years 1979–2005), which is similar to the findings of Roesch (2006) for CMIP3 models. Derksen and Brown (2012) further demonstrated, for a subset of eight  
60 CMIP5 models, that the models failed to capture the rapid decline in Northern Hemisphere late spring (May–June) snow cover observed in 2008–2012.

Regarding the reasons for biases in modeled snow conditions, the intercomparison studies have, in general, not been very conclusive. Most attention has been paid to biases in simulated air temperature (Foster et al., 1996; Räisänen, 2008) and total precipitation or  
65 snowfall (Foster et al., 1996; Roesch, 2006; Brutel-Vuilmet et al., 2013). Frei et al. (2005) further suggested that the exclusion of subgrid-scale treatments for terrain and land cover contributed to overestimated ablation rate of snow in spring over North America in AMIP2 models.

Multi-model intercomparisons have also demonstrated that the strength of snow-albedo  
70 feedback (SAF) varies substantially among both CMIP3 (Hall and Qu, 2006; Qu and Hall, 2007; Fletcher et al., 2012) and CMIP5 models (Qu and Hall, 2014). There is a strong correspondence between the SAF evaluated based on transient climate change experiments and based on the seasonal cycle. Model results for the seasonal SAF fall on both sides of the corresponding observational estimates (Hall and Qu, 2006; Fletcher et al., 2012;  
75 Qu and Hall, 2014). The simulated SAF is strongly influenced by the climatological surface albedo of snow-covered land, which shows a surprisingly large spread even among the CMIP5 models. Presumably, this is related to how vegetation masking of snow-covered land is treated (Qu and Hall, 2007, 2014).

The focus of the current work is narrower than in the multi-model intercomparisons discussed above, which, however, allows for more in-depth analysis. We look in detail at the  
80 performance of a single model, the ECHAM5 atmospheric GCM (Roeckner et al., 2003,

2006) in simulating the timing of snow melt in spring in Northern Eurasia, north of latitude  $55^{\circ}$  N. Specifically, we focus on the average timing of the end of the snow melt season (i.e., the snow-off date; the day when all snow accumulated during the winter has vanished). Snow-off dates simulated by ECHAM5 are compared with snow-off dates derived from two observational datasets: first, a satellite dataset based on data from passive multichannel microwave radiometers (Takala et al., 2009), and second, Russian in-situ snow course measurements (Bulygina et al., 2011a). The geographical focus on Northern Eurasia is motivated by the vast area of the continent, which makes Eurasian snow conditions important for understanding the planetary climate as a whole.

The performance of a slightly earlier version of ECHAM5 in simulating the Northern Hemisphere snow depth, snow-covered area and surface albedo was assessed by Roesch and Roeckner (2006). By using snow products based on visible and microwave remote sensing data, they found that ECHAM5 reproduces the amplitude and phase of the annual snow depth cycle quite precisely, however, with a slight overestimation of the snow depth in late winter and spring over Eurasia. The present work builds on Roesch and Roeckner (2006) but goes deeper in analyzing the regional details and causes underlying the biases in modelled snow-off dates. Thus, while it is shown that in ECHAM5 simulations, snow-off tends to occur too late in the eastern part of Northern Eurasia (especially southeastern Siberia) and too early in the western and northern parts, the most fundamental issue is that snow-off occurs at lower-than-observed air temperatures. The likely main reason for this are simplifications inherent to the model's surface energy budget calculation in the presence of partial snow cover and in the treatment of forest canopy. This highlights the need to consider carefully the treatment of the surface energy budget in the models, in addition to the fidelity of simulated temperature and precipitation fields.

The rest of this paper is organized as follows. First, in Sect. 2 we introduce the ECHAM5 model and the experiments conducted. In Sect. 3, the observational datasets used in this work are described. Section 4 addresses the non-trivial issue of the definition of snow-off dates. Results are reported in Sect. 5, both for the default version of ECHAM5 and for sensitivity experiments, in which biases in simulated atmospheric circulation were corrected

through nudging and/or the treatment of surface albedo was modified. The reasons underlying the biases in modeled snow-off dates are further discussed in Sect. 6, followed by conclusions in Sect. 7.

## 2 Model and experiments

### 2.1 Model description

Version 5.4 of the ECHAM5 atmospheric general circulation model (Roeckner et al., 2003, 2006) was used. The dynamical part of ECHAM5 is formulated in spherical harmonics, while physical parameterizations are computed in grid point space. The simulations reported were conducted at horizontal resolution T63 (corresponding to a grid-spacing of  $1.875^\circ$ ) with 31 layers in the vertical and model top at 10 hPa. A semi-implicit time integration scheme is used for model dynamics with a time step of 12 min. Model physical parameterizations (Roeckner et al., 2003) are invoked at every time step, except for radiation, which is computed once in two hours.

The snow scheme in ECHAM5 is relatively simple: the snow water equivalent (SWE;  $\text{kg m}^{-2}$ ) is a prognostic quantity, but changes in snow density or grain size are not considered. In the presence of snow, the top of the snow layer is treated as the top of the soil model. For snow-free and snow-covered land alike, the surface temperature is determined through the surface energy balance, while the thermal diffusion equation is used to calculate the soil (or snow) temperature profile. Five layers within the topmost 10 m are considered, with thicknesses of 0.065 m, 0.254 m, 0.913 m, 2.902 m and 5.700 m, respectively. For snow-free land, spatially varying volumetric heat capacity and thermal diffusivity are prescribed for five soil types according to the FAO soil map (Gildea and Moore, 1985; Henderson-Sellers et al., 1986). For snow-covered land the procedure is the same except that the thermal properties are modified. For example, if snow fills the top soil layer completely, and the second layer partially, the thermal properties of snow are used for the top

layer while a mass-weighted mixture of soil and snow properties is used for the second layer. A constant snow density of  $330 \text{ kg m}^{-3}$  is assumed in this procedure.

The ECHAM5 snow scheme considers both SWE intercepted by the canopy (Roesch et al., 2001) and SWE on the ground (Roeckner et al., 2003). The budget equation for snow on the ground accounts for snowfall through the canopy, sublimation/deposition, melting, and unloading of snow from the canopy due to wind. The snow melt rate  $M$  is computed from the surface energy budget equation:

$$C_L \frac{\partial T_s}{\partial t} = R_{\text{net}} + H + \text{LE} + G - M, \quad (1)$$

where  $C_L$  is the heat capacity of the surface layer,  $T_s$  the surface temperature,  $R_{\text{net}}$  the surface net radiation,  $H$  the sensible heat flux, LE the latent heat flux, and  $G$  the ground heat flux (all defined positive when the surface layer gains energy). A preliminary estimate for  $T_s$  at the next time step ( $T^*$ ) is obtained by considering everything else but snow melt ( $M = 0$ ). If  $T^*$  exceeds the melting point ( $T^* > T_0 = 0^\circ\text{C}$ ), the snow melt rate is inferred from the condition that the heat consumed in melting snow restores  $T_s$  to  $T_0$ :

$$M = \frac{C_L}{L_f} \left( \frac{T^* - T_0}{\Delta t} \right), \quad (2)$$

where  $L_f$  is the latent heat of fusion and  $\Delta t$  the model time step.

The snow cover fraction on the ground (SCF) is diagnosed following Roesch et al. (2001):

$$\text{SCF} = 0.95 \tanh(100h_{\text{sn}}) \sqrt{\frac{1000h_{\text{sn}}}{1000h_{\text{sn}} + 0.15\sigma_z + \epsilon}}, \quad (3)$$

where  $h_{\text{sn}}$  is SWE expressed in metres of liquid water,  $\sigma_z$  (m) is the subgrid-scale standard deviation of surface elevation and  $\epsilon$  is a small number used to avoid division by zero for totally flat and snow-free grid cells.

The parameterized grid-mean surface albedo depends on the specified background albedo, the fractional forest area of the grid cell, the snow cover on the canopy, the snow

cover on the ground, and a specified snow albedo. While a complete description of the parameterization can be found in Roeckner et al. (2003), two details are mentioned here to provide a background for the sensitivity tests in Sect. 2.2.3. First, the albedo of snow on land ( $\alpha_{\text{sn}}$ ) depends on the surface temperature  $T_s$  according to

$$\alpha_{\text{sn}} = \alpha_{\text{sn, min}} + (\alpha_{\text{sn, max}} - \alpha_{\text{sn, min}}) f(T_s) \quad (4)$$

where

$$f(T_s) = \min \left[ \max \left( \frac{T_0 - T_s}{T_0 - T_d}, 0 \right), 1 \right] \quad (5)$$

and  $\alpha_{\text{sn, min}} = 0.3$ ,  $\alpha_{\text{sn, max}} = 0.8$ ,  $T_0 = 0^\circ\text{C}$  and  $T_d = -5^\circ\text{C}$ . Second, the albedo of snow-covered forests is parameterized according to

$$\alpha_{\text{for}} = \text{SVF} \alpha_{\text{g}} + (1 - \text{SVF}) \alpha_{\text{can}}, \quad (6)$$

where  $\alpha_{\text{g}}$  is the ground albedo ( $\alpha_{\text{g}} = \alpha_{\text{sn}}$  if the ground is completely snow-covered),  $\alpha_{\text{can}}$  is the albedo of the canopy (0.2 for completely snow-covered canopy) and the sky view factor SVF depends on the leaf-area index (LAI):

$$\text{SVF} = e^{-\text{LAI}}. \quad (7)$$

## 2.2 Experiments

A total of six ECHAM5 experiments were conducted. All experiments were run for years 1978–2006, and years 1979–2006 were used for analysis of the results. Note that the years 2008–2012 during which a rapid reduction in Northern Hemisphere May–June snow cover has been observed (Derksen and Brown, 2012) fall outside this period. All simulations used observed sea surface temperatures (SST) and sea ice (AMIP Project Office, 1996), and some of them used nudging fields and/or observed albedo fields that likewise included “real” year-to-year variations (see below). The concentrations of well-mixed greenhouse gases

were held constant following AMIP II guidelines (AMIP Project Office, 1996), at 348 ppmv for CO<sub>2</sub>, 1650 ppbv for CH<sub>4</sub>, 306 ppbv for N<sub>2</sub>O, 280 pptv for CFC-11, and 484 pptv for CFC-12. For aerosols, a climatological distribution was assumed (Tanré et al., 1984). The distribution of ozone, vegetation area and LAI followed a prescribed climatological seasonal cycle.

Three of the experiments (REF, ALB1 and ALB2) were run in an ordinary climate simulation mode. In the remaining three experiments (REF\_NDG, ALB1\_NDG and ALB2\_NDG), four model fields were nudged towards ERA-Interim reanalysis data (Dee et al., 2011): vorticity (relaxation time scale 6 h), divergence (48 h), atmospheric temperature (24 h) and logarithm of surface pressure (24 h). Nudging acts to minimize the errors in simulated atmospheric circulation, which is one of the possible causes for differences between simulated and observed snow-off dates.

### 2.2.1 REF and REF\_NDG

The reference experiment (REF) and the corresponding nudged experiment (REF\_NDG) used the default version of ECHAM5.4. To evaluate the impact of model internal variability on the results, three runs were conducted for the REF experiment. The runs were started from different initial dates (1, 2 and 3 January 1978, respectively), which is sufficient for ensuring that within a few weeks, the weather conditions in the three runs become essentially independent of each other. Where not otherwise stated, the mean value of these three runs is reported. REF\_NDG, as well as ALB1, ALB1\_NDG, ALB2 and ALB2\_NDG consist of a single run for years 1978–2006.

### 2.2.2 ALB1 and ALB1\_NDG

Surface albedo influences strongly the energy available for melting snow in spring. In an attempt to eliminate errors in surface albedo, in the experiments ALB1 and ALB1\_NDG the model's albedo field over continents was replaced by prescribed surface albedos based on observations. Monthly-mean albedos in the CLARA-SAL dataset derived from AVHRR satellite data (Riihelä et al., 2013) were applied. Since this dataset starts from year 1982,

215 for years 1978–1981 the average annual cycle of CLARA-SAL albedo for years 1982–2006  
was employed. While this approach is instructive for diagnostic purposes, it has the major  
weakness that the albedo is independent of simulated land-surface properties, including  
snow cover.

### 2.2.3 ALB2 and ALB2\_NDG

220 In an attempt to reduce biases in ECHAM5's surface albedo field while keeping it interactive,  
experiments ALB2 and ALB2\_NDG were conducted. Two modifications were implemented  
in ECHAM5's surface albedo parameterization. First, for snow-covered forests, the sky-view  
factor in Eq. (7) was replaced by

$$\text{SVF} = e^{-(\text{LAI} + \text{SAI})} \quad (8)$$

225 Here, the stem area index (SAI) assumes a constant value of 2 for all forest types, follow-  
ing the Biosphere–Atmosphere Transfer Scheme (Dickinson et al., 1993). This modification  
was motivated by Roesch and Roeckner (2006), who noted that ECHAM5 overestimates  
the total surface albedo in eastern Siberia in the dormancy season of deciduous needleleaf  
230 trees, and ascribed this problem to the fact that the shadowing of the ground below the  
canopy by stems and branches is neglected. Second, the value of  $\alpha_{\text{sn}, \text{min}}$  in Eq. (4) was in-  
creased from 0.3 to 0.6. This was motivated by the findings of Pedersen and Winther (2005)  
and Mölders et al. (2008), who note that for ECHAM5's snow albedo parameterization, and  
also for ECHAM4 for which  $\alpha_{\text{sn}, \text{min}} = 0.4$ , snow albedo decreases too early and too fast  
during snowmelt.

## 235 3 Observational data

Seven observational datasets were used in the present work. First, a snow-off date dataset  
based on remote sensing of snow with space-borne microwave radiometer measurements  
(Takala et al., 2009) was used for evaluating snow-off dates in the ECHAM5 simulations.

240 The Eurasian region is well suited for remote sensing of snow melt for two reasons. First, temperatures in much of the Eurasian region are very low in winter-time, which leads to the formation of a dry snow pack. Second, as tundra is the predominant surface type, the snow conditions are relatively homogeneous over extended areas in the absence of e.g. mountain regions with a complicated topography. These properties are profitable for microwave instruments that measure highly contrasting surface brightness temperatures for dry vs. melting snow related to the progression of spring.

245 The remote-sensing dataset utilized measurements by the Scanning Multichannel Microwave Radiometer (SMMR; Knowles et al., 2002) onboard Nimbus 7 for years 1978–1987 and measurements by the Special Sensor Microwave/Imager (SSM/I) (Armstrong et al., 1994) onboard the Defence Meteorological Satellite Program (DMSP) satellites D-11 and D-13 for years 1988–2007. A time-series thresholding algorithm based on the brightness temperature difference between vertically polarized radiances around 37 GHz and 19 GHz was used to determine the snow-off date for each year (see Takala et al., 2009 for details). The snow-off dates (given as day-of-year from 1 to 180) are provided at a nominal resolution of 25 km × 25 km.

255 The snow-off date estimates in the microwave dataset were calibrated against the INTAS-SCCONE observations (Kitaev et al., 2002; Heino and Kitaev, 2003) of snow depth and snow melt flag at Eurasian, mostly Russian, weather stations. Specifically, for the calibration data, the snow-off date was defined as the last event during spring when the station snow status flag changed from “snow depth is correct” to “temporary melting” or “continuous melting”, both of which refer to a situation in which there is no snow left at the station. Thus, in principle, the microwave dataset is targeted at presenting the final snow-off date at each station. This is discussed further in Sect. 4.

265 Second, snow course measurements made in Russia (or the former Soviet Union) were used for evaluating both the simulated snow-off dates and the seasonal cycle of SWE. These data were acquired from the Russian Hydrometeorological Centre; <http://meteo.ru/english/climate/snow1.php> (Bulygina et al., 2011a). The “routine snow surveys” dataset contains data from 517 meteorological stations (288 within the region con-

sidered here), for which either open-terrain<sup>1</sup> or forest snow course measurements (or both) have been performed. These are a subset of the 958 stations considered in Bulygina et al. (2011b).

The SWE was measured at 100 meter intervals along the forest snow courses, which had a total length of 1 km, and at 200 meter intervals along the open-terrain snow courses with a total length of 2 km. Typically, measurements are provided at 10 day intervals in winter and 5 day intervals in spring (starting from March or April). The data availability varies, however, and not all stations provide data throughout the period 1979–2006 considered here. To compare with ECHAM5, the SWE values were regridded to the T63 grid, by averaging the SWE values over the stations if several stations existed in a grid cell. The procedure for estimating the snow-off date from the snow course data is described in the Appendix. We include in our analysis those grid cells for which the snow-off date could be determined for at least five years during 1979–2006.

Third, for surface albedo, we employ the monthly mean version of the CLARA-SAL dataset (Riihelä et al., 2013), which is based on a homogenized AVHRR radiance time-series. These data provide black-sky albedo values from January 1982 onwards. The data, originally given at a  $0.25^\circ \times 0.25^\circ$  resolution, were averaged to the T63 grid for comparison with modelled values, and for use as input for the ALB1 and ALB1\_NDG experiments (Sect. 2.2.2).

Fourth, for snow cover fraction, we use version 2.0 of the snow extent (SE) dataset created in the European Space Agency’s (ESA) Data User Element project GlobSnow (Metsämäki et al., 2015). The GlobSnow SE is based on data acquired by the ERS-2/ATRS-2 and Envisat/AATSR satellite instruments, and is provided on a  $0.01^\circ \times 0.01^\circ$  grid. Here, monthly-mean data averaged to the T63 grid are used. The years for which there is spring-time snow cover data both for GlobSnow and the current ECHAM5 experiments are 1997–2006, but 2002 was discarded due to issues with data quantity and quality. While longer-

---

<sup>1</sup>The term “open-terrain snow courses” is used here instead of the term “field snow courses” used in Bulygina et al. (2011a, b). These refer to non-forested snow courses in general, some of which are above (or north of) the treeline.

295 term snow cover datasets exist (Zhao and Fernandes, 2009; Brown and Robinson, 2011),  
GlobSnow was selected for the present study because its retrieval algorithm was specifi-  
cally designed to enable accurate snow mapping also in forests, which cover a large part of  
Northern Eurasia.

300 Fifth, information on forest cover from the GlobCover 2009 dataset (Bontemps et al.,  
2011; Arino et al., 2012) is used, along with the GlobSnow snow cover data, to aid the  
interpretation of the differences between modelled and observed albedo fields.

Sixth, for 2 m air temperature, Climate Research Unit (CRU) land surface air temperature  
data, version 3 (CRUTEM3; Brohan et al., 2006) is employed.

305 Seventh, daily measurements of snow depth and diurnal-mean temperature conducted  
at the Finnish Meteorological Institute Arctic Research Centre at Sodankylä (67.37° N,  
26.63° E, 179 m a.s.l.) in January–June 1979–2006 are employed for a detailed compar-  
ison with ECHAM5 experiments in Sect. 6. The Sodankylä site belongs to the northern  
boreal forest zone with the snow type of taiga, which is typical of most of Northern Eurasia.

#### 4 Definition of snow-off date

310 Snow-off date is evaluated in ECHAM5 based on daily-mean SWE values. There are several  
possible methods for defining the snow-off date, the most obvious ones being (1) the first  
snow-off date (i.e., the first day with zero SWE after a winter's SWE maximum) and (2) the  
final snow-off date (i.e., the day following the last day with SWE > 0 in spring). In some  
cases, the first and final snow-off dates differ substantially. As an example, Fig. 1 shows the  
time series of SWE for spring 1988 for a grid point in western Russia (60.6° N, 39.4° E) in  
315 one of the REF runs. The first snow-off date is day 99 (8 April), but three separate short  
periods with snow occur after it, the final snow-off date being day 129 (8 May).

In this paper, we use the first snow-off date for ECHAM5 because it is a more robust  
indicator of model behavior than the final snow-off date. The first snow-off date represents  
an integral measure of how much snow accumulates during the winter and how fast it melts  
320 in the spring. In contrast, when the final snow-off date differs from the first snow-off date,

it is, in essence, determined by the last occurrence of solid or mixed-phase precipitation in spring. This makes the final snow-off date much more sensitive to day-to-day weather patterns in spring than the first snow-off date.

Even when setting aside potential issues related to spatial and temporal resolution, the definition of snow-off date in ECHAM5 results is not fully compatible with how the snow-off date is derived from the microwave satellite data. As noted in Sect. 3, the satellite snow-off date represents, in principle, the final snow-off date rather than the first snow-off date; that is, it can be affected by secondary periods of snow after the first snow-off date. Nevertheless, the use of final snow-off date in ECHAM5 for comparison with the satellite data would be problematic. The secondary periods of snow after the first snow-off date in ECHAM5 are often short and the values of SWE very low (e.g.,  $SWE \sim 0.1 \text{ kg m}^{-2}$  for the last two periods of snow in Fig. 1) so it is unclear whether they would really be detected by the satellite algorithm. Thus, we opt to use the first snow-off date for ECHAM5, but acknowledge that this may contribute towards an early bias in snow-off dates when compared with the satellite data.

In the comparisons with the snow course data, the snow-off date in ECHAM5 is evaluated as the first snow-off date, but using SWE for only those days for which snow course measurements are available (i.e., every 5th or 10th day). This is fully consistent with how the snow-off date is derived from the snow course data (see the Appendix).

Figure 2 compares time-average snow-off dates derived from the snow course data and the satellite data, for each ECHAM5 grid cell separately. While these estimates are, of course, strongly correlated ( $r=0.775$ ), there is an appreciable scatter among them. For some grid cells, the difference between satellite and snow-survey snow-off dates is more negative than  $-10$  days, and for many more grid cells (especially in Siberia, in particular between  $100^\circ \text{ E}$  and  $120^\circ \text{ E}$ ) more positive than 10 days. The mean difference between the satellite and snow survey snow-off dates is 5.1 days, while the rms difference is 12.2 days. The positive mean difference is, in principle, consistent with the notion that the satellite snow-off date may be in some cases influenced by secondary periods of snow after the first snow-off date; however, the substantial scatter indicates that there must be other

350 factors at play. Unraveling the causes of these differences falls beyond the scope of this paper. Rather, we focus on what can be concluded from the model behaviour, given the observational uncertainty.

## 5 Results

### 5.1 Reference experiment REF

#### 355 5.1.1 Snow-off timing

The geographical distribution of the mean snow-off date during the period 1979–2006 in the satellite retrievals is shown in Fig. 3a. In general, springtime snow-off progresses gradually from the southwestern parts of the domain towards the northern and eastern parts. Earliest snow-off occurs in the Baltic Sea area (around 20° E), before day 90 (end of March). An area of rather early snow-off dates can also be found in eastern Siberia where around the latitude 60° N snow melts right after day 120 (beginning of May). Snow melts latest in the Taymyr Peninsula (around 75° N, 100° E), after day 170 (about 20 June). Snow also persists until June in parts of Russian Far East (east of 160° E). In addition to the general southwest-to-northeast gradient, some orographic effects can be detected. In the Ural Mountains (60° E) and in the Scandinavian (about 20° E) and Verkhoyansk (130° E) mountain ranges, snow melts later than in the surrounding regions, by up to 30 days in the Ural region. Although mountainous areas are problematic to handle in algorithms based on microwave radiometer data (Mialon et al., 2008; Pulvirenti et al., 2008), these features are expected on physical grounds: colder temperatures and orographically enhanced precipitation favour later snow melt.

370 The REF experiment (Fig. 3b) reproduces well the general pattern of snow-off dates seen in the satellite data, the snow-off being latest in the Taymyr Peninsula (between days 150 and 160) and earliest in the Baltic Sea region (around day 80). However, in most of Northern Eurasia, snow melts earlier in the model results than in the satellite retrievals

375 (Fig. 3c). The difference to the satellite retrievals is mainly 5–20 days but locally exceeds  
20 days in Northern Europe. On the contrary, in eastern Siberia and in some far eastern  
parts of Russia, snow melts locally over 10 days later in REF than in the satellite data. The  
orographic effects seen in Fig. 3a are absent in the model results, presumably because the  
model resolution (T63) is too coarse for describing them.

380 Figure 3d displays the standard deviation in the 28 year mean (1979–2006) snow-off date  
among the three runs included in the REF experiment. For most of Northern Eurasia, the  
standard deviation is less than 2 days, with larger values mainly confined to the southwest-  
ern part of the domain and the Scandinavian coastline. In general, the standard deviation  
is much smaller than the respective differences between REF and the satellite data. This  
385 provides a justification for including only a single model run in the sensitivity experiments.  
Finally, Fig. 3e and f show the interannual standard deviation of snow-off dates for the satel-  
lite retrievals averaged to the model grid and for the REF simulation, respectively. Overall,  
the magnitude and the geographic pattern of the standard deviation are similar for the model  
results and for the observations, typical values ranging from 5–6 days in central and eastern  
390 Siberia to  $\sim 20$  days in the Baltic Sea region. Naturally, there are some differences in the  
details, such as, for example, a smaller standard deviation of snow-off dates in REF than in  
the satellite dataset in western Siberia.

Figure 4a compares the snow-off dates in the REF experiment with those derived from  
the snow course data. The general tendency towards too early snow-off dates in the west  
395 (about 30–90° E) and too late snow-off dates in the east in REF as compared with the snow  
course data is in qualitative agreement with the corresponding comparison with satellite  
data (Fig. 3c). However, the positive differences in the east, indicating delayed snow-off in  
ECHAM5, are more widespread and more pronounced than those in Fig. 3c, exceeding 20  
days at some locations. Figure 4b and c show a similar comparison as Fig. 4a, but sepa-  
400 rately for open-terrain and forest snow courses. It is seen that particularly in the west, the  
model snow-off dates are rather close to those derived from the open-terrain snow courses,  
the differences being only slightly negative, and in some cases slightly positive. In contrast,  
a comparison with the forest snow courses west of 90° E shows a persistent negative bias,

405 indicating too early snow melt in the model. The more negative differences for the forest  
snow courses than for the open-terrain courses indicate that snow tends to persist longer  
in forests than on open ground. For those grid cells (located mainly in western Russia) that  
have both forest and open-terrain courses, the snow clearance occurs on average 10.5 days  
later for the forest courses. In ECHAM5, however, neither snow-off dates nor SWE values  
are defined separately for the forested and non-forested parts of a grid cell.

410 The later snow-off for forests is consistent with the findings of Lundquist et al. (2013) for  
locations with cold winters (December-January-February (DJF) mean temperatures colder  
than  $-6^{\circ}\text{C}$ , which applies to most of Northern Eurasia). However, the opposite behaviour  
(earlier snow-off in forests than on open ground) was observed in climates with warm win-  
415 ters (DJF mean temperature  $> -1^{\circ}\text{C}$ ). In general, several factors influence the relative  
timing of snow-off in forests and on open ground (e.g., Essery et al., 2009; Strasser et al.,  
2011). During the accumulation season, the interception and subsequent sublimation of  
canopy snow reduces accumulation of snow in forests, while wind-blown snow from open  
areas may be deposited around forest edges, thus increasing the snow depth. In spring,  
420 less solar radiation is available for melting the snow under a forest canopy than on open  
ground, but increased downwelling longwave radiation may partly compensate for this.

### 5.1.2 Other snow-related quantities

To set the stage for further discussion, 2 m air temperature ( $T_2$ ), surface albedo, SCF and  
SWE are considered. Figure 5 shows a comparison of  $T_2$  in REF and in the CRU data for  
the extended spring season (March through June). A cold bias prevails through most of  
425 the spring and peaks at  $-7\text{ K}$  in southeastern Siberia in April. Positive temperature biases  
occur in the Taymyr region (throughout the spring) and in the Russian Far East (mainly in  
March and April).

The left half of Fig. 6 displays a comparison of surface albedo in the REF experiment  
with the CLARA-SAL dataset. Two pronounced biases appear. First, in agreement with  
430 Roesch and Roeckner (2006), a positive bias prevails in the central and eastern parts of  
Siberia for much of the spring, especially in March and April. Second, a negative albedo

bias occurs in the northernmost parts of Northern Eurasia (especially in the Taymyr region) in May and June, and in northern Fennoscandia especially in April. Some understanding of the albedo biases can be gained by considering the snow cover fraction along with forest fraction and LAI.

The right half of Fig. 6 shows monthly-mean SCF differences between the REF simulation and the GlobSnow dataset for the years 1997–2006, excluding 2002. Although this period is shorter than the period 1982–2006 used for the albedo comparison, the REF vs. CLARA-SAL albedo differences for these two periods are very similar, with monthly spatial correlations of 0.98–0.99. Interestingly, ECHAM5 underestimates SCF compared to GlobSnow almost throughout the Northern Eurasia, with the exception of parts of southeast Siberia in May, where snow-off is delayed in the REF simulation. During March and April, the GlobSnow SCF is very high (0.99–1) through much of the central and northern parts of Northern Eurasia. For ECHAM5, SCF is typically 0.90–0.95 in non-mountainous regions, but locally only  $\approx 0.75$ –0.8 in the Verkhoyansk range in Eastern Siberia, where SWE is relatively low (60–80 kg m<sup>-2</sup>) and subgrid orographic variability is fairly large,  $\sigma_z \approx 250$  m (see Eq. (3)). The largest negative SCF differences to GlobSnow occur, however, in the snowmelt season, in April and May in the western parts of Northern Eurasia and in June in the Taymyr peninsula, consistent with the too early snow-off in these regions. The small negative SCF biases that appear in June in southern and western parts of Northern Eurasia in Fig. 6h are, however, artifacts related to clouds misinterpreted as snow in the GlobSnow dataset.

The impact of SCF biases on surface albedo is best discernible in tundra (i.e., forest-free) regions (see Fig. 7a,b for the distribution of forests). In particular, the strong negative albedo bias in June in the Taymyr peninsula in Fig. 6g is related to insufficient snow cover in the REF simulation. The negative albedo bias in the northernmost parts of Fennoscandia and Russia in May can also be partly ascribed to underestimated SCF. However, especially in the Taymyr peninsula, the albedo bias ( $\approx -0.24$ , averaged over land grid points north of 72.5° N) is larger than the SCF bias ( $\approx -0.12$ ). Very likely, this is related to the unrealistically low value (0.3) assumed for the albedo of “warm” snow ( $T_s \geq 0^\circ\text{C}$ ).

The positive albedo bias that prevails in central and eastern Siberia (and to a lesser extent, in parts of western Russia) in March and April is related to the treatment of forests. Indeed, the regions with most pronounced positive albedo bias are associated with a high forest fraction (locally higher than 0.9) in the GlobCover 2009 dataset (Fig. 7a). In ECHAM5, the forest fraction is somewhat smaller, typically  $\approx 0.5$ – $0.6$ . This difference should be interpreted with caution, however, as the dominant GlobCover land cover class in forested parts of Siberia is “open needleleaved deciduous or evergreen forest”, which has a canopy coverage of 15%–40% when viewed from directly above. The reason why the albedo bias is especially large in central and eastern Siberia is related to the LAI. There, the LAI in ECHAM5 is very low in the dormancy season of deciduous needleleaf trees, including March and April (Fig. 7c). When only the leaves (and not the stems and branches) are considered in the computation of the sky-view factor (Eq. (7)), this results in very little shading of the snow surface by the forest. Therefore, as previously discussed by Roesch and Roeckner (2006), the albedo is overestimated substantially.

Figure 8 shows the average annual cycle of SWE in the REF experiment and in the snow course measurements, for the entire Northern Eurasia and for two subregions denoted as Western Russia ( $55$ – $70^\circ$  N,  $30$ – $70^\circ$  E) and Eastern Siberia ( $55$ – $70^\circ$  N,  $100$ – $140^\circ$  E). Note that grid cells without snow course data are not included in the averages, and therefore, for example, the average over the entire Northern Eurasia gives more weight to the western and southern parts of the region than its eastern and northern parts, especially when considering open-terrain snow courses. With this caveat in mind, we note that the domain-mean annual cycle of SWE over the entire Northern Eurasia in REF agrees well with the snow course data, although the maximum is slightly higher and occurs 5–10 days earlier than observed (Fig. 8a). There are, however, regional differences. For Western Russia (Fig. 8b), the simulated maximum SWE is very close to that observed, but SWE starts to decrease earlier than observed in the spring, in agreement with the too early snow-off days in Figs. 3c and 4a. In contrast, for Eastern Siberia, the REF experiment overestimates substantially the accumulation of snow during winter (Fig. 8c), and the timing of maximum SWE and snow melt is delayed, which is again consistent with Fig. 4a.

490 When considering the open-terrain snow courses only, the simulated SWE maximum is  
higher than observed for all three regions (Fig. 8d–f), and the overestimate is especially pro-  
nounced for Eastern Siberia. In contrast, when compared with the forest snow courses, the  
simulated maximum SWE is slightly too low for the entire Northern Eurasia (Fig. 8g) and for  
Western Russia (Fig. 8h) and only moderately overestimated for Eastern Siberia (Fig. 8i).  
495 The more positive ECHAM5 vs. observation differences for open-terrain than forest snow  
courses suggest that in reality (but not in ECHAM5), more snow accumulates in forests than  
on open ground. We verified that this also holds true when the comparison is restricted to  
grid cells and years with both forest and open-terrain observations. It is worth noting that  
often the opposite has been reported (though mainly for sites at lower latitudes): less accu-  
500 mulation in forests due to sublimation of intercepted snow or due to midwinter melt induced  
by the larger downwelling longwave flux in forests (Essery et al., 2009; Strasser et al., 2011;  
Lundquist et al., 2013).

The delayed snow-off in the REF experiment in central and eastern Siberia is physically  
consistent with the low temperature bias and high albedo bias in spring. On one hand,  
505 overestimated surface albedo keeps the absorbed solar radiation low, which favours cold  
temperatures and delays the onset of snow melt. On the other hand, delayed snow melt  
provides a positive feedback by keeping the albedo high. Furthermore, too large accumu-  
lation of snow in winter contributes to the delayed snow-off in Eastern Siberia (Fig. 8c).  
Similarly, underestimated albedo and overestimated  $T_2$  in spring in the Taymyr region are  
510 consistent with the snow vanishing too early. For Western Russia, however, the main rea-  
son for the earlier than observed snow-off dates (Figs. 3c and 4a) seems to be that at least  
in a domain-average sense, snow melt starts somewhat too early (Fig. 8b). Intriguingly, this  
occurs in spite of a slightly negative temperature bias in spring (Fig. 5).

## 5.2 Sensitivity experiments

515 The sensitivity experiments show that both nudging and changes in the treatment of sur-  
face albedo have substantial impacts on the snow-off date simulated by ECHAM5 (Fig. 9).  
Nudging makes snow-off occur earlier in most of Northern Eurasia, with largest effect

(over 15 days) in southeastern Siberia and locally in Fennoscandia. The earlier snow-off in REF\_NDG is both due to higher temperatures (as discussed below) and due to slightly  
520 reduced snowfall in eastern Siberia, as reflected in the seasonal cycle of SWE in Fig. 8c, f and i. However, in the Taymyr region, snow-off is delayed by more than 5 days in REF\_NDG as compared with REF (Fig. 9a). Use of observed (CLARA-SAL) albedo in ALB1 likewise makes the snow melt earlier in southeastern Siberia and later in the Taymyr region, with larger impact in the latter (ALB1–REF differences of  $\approx -5$  days and  $\approx 15$  days, respectively; Fig. 9b). In general, snow-off is delayed somewhat in the northern parts of Northern Eurasia, and also in central Russia. For the ALB2 experiment with changed albedo parameterization, snow-off occurs up to 5 days earlier in southeastern Siberia than in REF (Fig. 9c). This is very similar to the ALB1 experiment, and results from the modification of the sky-view factor in the calculation of surface albedo in forested regions. However, due to the increase of the albedo of “warm” snow ( $T_s \geq 0^\circ\text{C}$ ) from 0.3 to 0.6, snow-off is delayed  
530 in the northeastern parts of the Russian Far East and particularly in the Taymyr region, locally by 5–10 days. This response is qualitatively similar but somewhat weaker than that in ALB1. Finally, when nudging is combined with changed treatment of albedo (ALB1\_NDG and ALB2\_NDG; Fig. 9c and e), the earlier snow-off in southeastern Siberia and delayed snow-off in the Taymyr region become even more pronounced. In southeastern Siberia, the difference to REF reaches locally  $-20$  days.

Figures 10 and 11 compare the snow-off dates in all ECHAM5 experiments with the snow-off dates derived from microwave satellite data and Russian snow course data, respectively. In spite of the inter-experiment differences noted above, all free-running (i.e.,  
540 non-nudged) simulations show the same basic pattern of differences compared to the satellite data (Fig. 10): too early snow-off dates in the west, along with regions of delayed snow-off in eastern parts of northern Eurasia. The ALB1 and ALB2 experiments show some improvement in southeastern Siberia, where the positive bias in snow-off date is reduced but not eliminated. Furthermore, the negative bias in the Taymyr region is reduced in the ALB2 experiment with changed snow albedo parameterization, and turned into a slight positive bias in ALB1, which uses observation-based CLARA-SAL albedo data.

Nudging eliminates entirely the positive bias in snow-off date in southeastern Siberia as compared with the satellite data. As a consequence, the REF\_NDG experiment features an early bias throughout Northern Eurasia (Fig. 10b), with largest biases in the west. Likewise, for the nudged simulations with albedo changes (ALB1\_NDG and ALB2\_NDG), snow-off generally occurs earlier than in the satellite data, the most notable exception being that for ALB1\_NDG, near-zero or even positive differences (i.e., delayed snow-off) appear in the Taymyr region.

It should be recalled that the early bias in snow-off dates compared with the satellite data may be, in part, an artifact related to differences in the definition of snow-off time between the ECHAM5 simulations and the satellite data (Sect. 4). Indeed, when compared with the snow course data (Fig. 11), all free-running simulations feature delayed snow-off in eastern Siberia and in the Russian Far East. The differences between REF, ALB1 and ALB2 are rather small in comparison with their biases with respect to the snow course data. Even for the nudged simulations (REF\_NDG, ALB1\_NDG, and ALB2\_NDG), positive differences indicating delayed snow-off prevail for many measurement stations in Eastern Siberia and in the Russian Far East, although slightly negative differences occur for some stations. In the western parts of Northern Eurasia, however, all simulations feature negative biases, snow-off occurring 10–20 days earlier than in the snow course data for many stations in western Russia. The negative biases are, in general, slightly larger for the nudged simulations, especially in the westernmost parts of Russia. Furthermore, as noted in Sect. 5.1 for the REF experiment, the negative biases are especially pronounced when compared with forest snow courses.

The changes in snow-off timing are influenced by, and they feed back on, simulated 2 m air temperature (Fig. 12) and surface albedo (Fig. 13) in the sensitivity experiments. For brevity, only mean values over the months of April and May are shown. All experiments feature a cold bias in southeastern Siberia, which amounts down to  $-7$  K in REF (Fig. 12a). Consistent with the earlier snow melt (Fig. 9), this bias is reduced in ALB1 (Fig. 12c) and ALB2 (Fig. 12e), and especially in the nudged experiments (Fig. 12b, d and f). A slight negative temperature bias ( $\approx -2$  to  $-1$  K) prevails in large parts of western and central

Russia, and this feature varies only slightly between the experiments. Positive temperature biases are seen in all experiments in the Taymyr region and in parts of the Russian Far East.

580 Figure 13 displays surface albedo differences from the CLARA-SAL data for the REF, REF\_NDG, ALB2 and ALB2\_NDG experiments (for ALB1 and ALB1\_NDG, the differences are zero by construction). It is seen that the high albedo bias in southeastern Siberia is reduced substantially in both REF\_NDG and ALB2, and it is eliminated completely in ALB2\_NDG. In the case of ALB2 and ALB2\_NDG, the modified computation of the sky-view factor in the albedo parameterization for forested regions contributes to this. For REF\_NDG, 585 however, the change in surface albedo stems entirely from changes in meteorological conditions, the reduced negative temperature bias (Fig. 12b) leading to both lower snow albedo and reduced snow cover. However, all four experiments show some common biases, most distinctly an underestimation of albedo compared to the CLARA-SAL data in the northern parts of Northern Eurasia and in the Russian Far East. Interestingly, the use of a higher value for the albedo of “warm” snow (0.6 instead of 0.3 when  $T_s \geq 0^\circ\text{C}$ ) in the ALB2 and ALB2\_NDG experiments reduces somewhat the negative bias in the Taymyr region but does not eliminate it. A negative SCF bias likely contributes to the remaining albedo bias, the average difference to GlobSnow data in the Taymyr peninsula being  $\Delta\text{SCF} \approx -0.08$  both in April and May. However, it still appears that snow albedo is underestimated in May, 590 which suggests that even the value of 0.6 is too low at least in this region.

## 6 Discussion

The analysis of the sensitivity experiments in Sect. 5.2 showed that nudging and changes in the treatment of surface albedo in the presence of snow alleviated some of the model biases in snow-off dates, 2 m temperature and surface albedo. Nevertheless, many of the biases 600 seen in Figs. 10–13 are quite similar for all experiments. Regarding the timing of springtime snow-off, the results are somewhat ambiguous for the eastern parts of Northern Eurasia, due to large differences between observational snow-off date estimates from satellite and

snow course data, and hence in the resulting model biases. For western Russia, however, comparisons with the satellite data and the snow course data indicate unanimously that  
605 snow-off occurs too early in ECHAM5 for all experiments, with only moderate variations due to nudging or changes in the treatment of surface albedo (Figs. 10 and 11). Moreover, surprisingly, the too early snow-off co-occurs with a slight negative temperature bias in the snow-melt season (Fig. 12).

To shed more light on the seemingly contradictory biases in temperature and snow-off  
610 dates, a detailed comparison of ECHAM5 results with observations at Sodankylä in Finnish Lapland is presented. The black line in Fig. 14a displays the mean seasonal cycle of snow depth measured at Sodankylä in 1979–2006, for days of year 1–165 (i.e., from 1 January until 14 June). The other curves show the corresponding seasonal cycle of SWE for four ECHAM5 experiments (REF, REF\_NDG, ALB1 and ALB2). While there is no one-to-one  
615 correspondence between snow depth and SWE, due to variations in snow density, it is clear from Fig. 14a that in three of the four ECHAM5 experiments (REF, REF\_NDG and ALB2), snow melt occurs earlier than in the observations, by roughly 10–15 days. This is consistent with Fig. 3c, which indicates that in the Finnish Lapland, snow-off in the REF experiment occurs  $\sim 15$  days earlier than in the satellite data. The exception is that in the  
620 experiment ALB1, which prescribes surface albedo from the AVHRR-based CLARA-SAL dataset, the timing of snow melt coincides well with the observations.

Figure 14b shows a comparison for the seasonal cycle of 2 m air temperature. From mid-March (day 75) onwards, all ECHAM5 simulations underestimate the average  $T_2$  systematically. The average underestimate in the primary snow melt season (mid-April to mid-May; days 105–135), is  $\approx 1.8$  K for REF, REF\_NDG and ALB2, and  $\approx 3.5$  K for ALB1. Thus  
625 the Sodankylä site represents a case where snow melt (and snow-off) occurs earlier in ECHAM5 than in the observations, in spite of a negative temperature bias in the snow melt season.

The problems with representing correctly the relationship between snow melt timing and  
630 temperature become even more obvious, when the temperature data are composited with respect to the snow-off date. Thus, for each year in 1979–2006, the snow-off date (“day

0”) was defined as the first day after the winter’s snow maximum completely without snow (in ECHAM5) or with snow depth equal to zero in the morning (in the observations), and the average  $T_2$  was computed for each day in the range from 45 days before snow-off to 15 days after snow-off (Fig. 14c). Note specifically that as “day 0” represents the first completely snow-free day, snow actually vanishes sometimes during “day – 1”, and “day – 2” is (generally) the last day with snow persisting throughout the day.

It is clear from Fig. 14c that ECHAM5 substantially underestimates  $T_2$  in the snow melt season. Strikingly, this depends quite little on the experimental details such as nudging or changed treatment of surface albedo. The negative bias in  $T_2$  culminates just before snow-off, being  $\approx -7$  K on “day – 2”. Furthermore, it is noted that in ECHAM5, the average  $T_2$  reaches  $0^\circ\text{C}$  as late as “day – 1”, during which the snow vanishes in the model. In the observations, the average  $T_2$  reaches  $0^\circ\text{C}$  already on “day – 20”, and climbs to  $7^\circ\text{C}$  by “day – 1”. It is further seen that in ECHAM5, there is a substantial jump in temperature from “day – 2” (the last day with snow throughout the day) to “day 0” (the first completely snow-free day),  $2.9\text{--}3.9^\circ\text{C}$  depending on the experiment, whereas the observed change is only  $1.0^\circ\text{C}$ . A similar composite analysis of temperature with respect to snow-off date was repeated for ECHAM5 for the entire Northern Eurasia, and it confirmed that the behaviour seen in Fig. 14 is quite universal. In particular, throughout the region, the average  $T_2$  stayed below  $0^\circ\text{C}$  until and including “day – 2” (not shown).

The likely main reason for the fact that  $T_2$  simulated by ECHAM5 stays close to  $0^\circ\text{C}$  in the snow melt season is that the surface energy budget (and hence surface temperature) is not computed separately for the snow-free and snow-covered parts of the grid cell. Rather, while snow cover fraction is taken into account in defining grid-mean properties like surface albedo and roughness length, a single snow-covered energy balance computation is performed (Eq. 1).

As explained in Sect. 2.1, the amount of snow melt is determined from the condition that, when the surface temperature  $T_s$  would rise above  $0^\circ\text{C}$  without considering snow melt, the heat consumed in melting snow restores  $T_s$  to  $0^\circ\text{C}$  (Eq. 2). Here,  $T_s$  refers to the grid-mean surface temperature, not the temperature of melting snow. Therefore, as long as there is any

snow left in the grid cell,  $T_s$  is not allowed to rise above  $0^\circ\text{C}$ , irrespective of the snow cover fraction. Naturally, this acts to suppress the sensible heat flux (or even makes it negative), so 2 m air temperature cannot rise much above  $0^\circ\text{C}$  either. In reality, in a region with partial (patchy) snow cover, surface temperature is kept to zero only in the patches of melting snow. In the snow-free patches,  $T_s$ , and consequently,  $T_2$ , can rise substantially above  $0^\circ\text{C}$ . Furthermore, local temperature advection from snow-free to snow-covered patches and subsidence associated with a “snow breeze” circulation can increase  $T_2$  over the latter (e.g., Yamazaki, 1995; Liston, 1995).

In summary, the use of a single surface energy budget computation leads to a misrepresentation of grid-mean surface fluxes in the presence of fractional snow cover (Liston, 2004): too much energy is spent in melting snow, and too little in warming the air and the ground. Consequently,  $T_2$  stays too low in the snow melt season (Fig. 14c). This likely explains why ECHAM5 features a persistent cold bias in springtime  $T_2$  even in regions where snow-off occurs earlier than observed (Figs. 10–12).

In addition, there is another factor related to the treatment of surface energy budget that may contribute to the too early snow-off: ECHAM5 does not include a canopy layer. In ECHAM5, forests influence the energy budget through changing the surface albedo and roughness length, but, for example, the shading of the surface by the canopy is not considered. Since forests reduce the surface albedo in the presence of snow (or more precisely, the combined albedo of the surface and the canopy) in ECHAM5, this implies that the amount of solar radiation available for snow melt at ground is increased in forests. In reality, the opposite happens, which acts to delay springtime snowmelt in forests relative to non-forested areas (Strasser et al., 2011). This may explain why, in comparison with the snow course data, ECHAM5’s tendency toward too early snow-off is more pronounced for forest than open-terrain measurements (Fig. 4b–c).

Recently, Brutel-Vuilmet et al. (2013) found that, while there is still substantial intermodel dispersion among the CMIP5 models, on average the spring-time snow melt is slightly delayed in Northern Eurasia. Taken at face value, the default version of ECHAM5 agrees with this result for the eastern parts of Northern Eurasia, while in the west, snow van-

690 ishes too early (Figs. 3 and 4). However, such regional features are not discussed in  
Brutel-Vuilmet et al. (2013), and moreover, a rigorous comparison with their results is dif-  
695 ficult due to the different datasets and analysis methods used (e.g., Brutel-Vuilmet et al.,  
2013, used only monthly data). An interesting question for further research is how well the  
CMIP5 models are able to represent the relationship between spring-time temperature and  
snow-off timing. In particular, is the problem of snow melt occurring at too cold grid-mean  
700 temperatures, as demonstrated in the current study, an exception or the rule for the CMIP5  
models? A priori, we would expect some of the models to behave better (or at least dif-  
ferently) than ECHAM5. A prime example is the CLM4 land-surface model (Oleson et al.,  
2010) employed in the Community Earth System Model (CESM) (Hurrell et al., 2013), which  
addresses all the main limitations of ECHAM5 identified in this work: the energy budget  
computation is separated for the snow-covered and snow-free parts of a grid cell, the com-  
putation of radiative fluxes at the snow surface accounts for the shading by the overlying  
705 forest canopy, and the snow albedo computation is more rigorous, based on radiative trans-  
fer modelling and a prognostic effective radius of snow grains. The CLASS land surface  
scheme (Verseghy, 2000) used in the CanCM4 climate model (von Salzen et al., 2013) also  
separates the energy budgets for snow-covered and snow-free land.

## 7 Conclusions

710 In the present work, we have evaluated the timing of springtime snow-off in Northern Eura-  
sia in the ECHAM5 (version 5.4) atmospheric GCM. Simulated snow-off dates were com-  
pared with a snow-off date dataset based on space-borne microwave radiometer measure-  
ments and with Russian snow course data. The primary conclusions are as follows:

- In general, the default version of ECHAM5 reproduces well the observed geographic  
715 pattern of snow-off dates, with earliest snow melt (snow disappearing in March) in the  
Baltic region, and latest snow melt (in June) in the Taymyr region and parts of the  
Russian Far East. However, compared to the satellite data, snow-off occurs too early  
in the western parts of Northern Eurasia, and also in the northernmost regions like the

Taymyr peninsula, with largest differences (locally over 20 days) in Northern Europe. On the contrary, in southeastern Siberia and in some far eastern parts of Russia, snow melts locally over 10 days later than in the satellite data. Comparison with the Russian snow course data confirms the pattern of too early snow-off in the west and too late snow-off in the east, although the former is slightly less pronounced, and the latter more pronounced, than in the corresponding comparison with the satellite dataset.

- The later than observed snow-off in southeastern Siberia is associated both with overestimated snow accumulation during winter and a springtime cold bias, which exceeds  $-6$  K in April. The latter is, in part, related to an overestimation of surface albedo, which arises from insufficient shadowing of the snow surface by the canopy in ECHAM5 in the dormancy season of deciduous needleleaf trees. In contrast, surface albedo is underestimated in late spring especially in the Taymyr region, both due to underestimated snow cover and because an unrealistically low albedo (0.3) is assumed for “warm” snow ( $T_s \geq 0^\circ\text{C}$ ). This promotes too early snow-off in this region.
- Several sensitivity experiments were conducted, where biases in simulated atmospheric circulation were corrected through nudging and/or the treatment of surface albedo was modified. Both nudging and surface albedo modifications alleviated some of the model biases in snow-off dates, 2 m temperature ( $T_2$ ) and surface albedo. In particular, it proved possible to reduce substantially the biases in snow-off date in southeastern Siberia and in the Taymyr region. In contrast, the early bias in snow-off in the western parts of Northern Eurasia was not reduced appreciably in any of the experiments; rather it was slightly increased by nudging. Furthermore, surprisingly, this early bias in snow-off was accompanied by a slight negative bias ( $\approx -2$  to  $-1$  K) in springtime  $T_2$ , both for the default version of ECHAM5 and for the sensitivity experiments.
- The combination of a too early snow-off with a cold springtime temperature bias implies that temperature stays too low in the snow melt season. In fact, as long as there is any snow left on the ground, the daily-mean  $T_2$  simulated by ECHAM5 rarely rises

745 above  $0^{\circ}\text{C}$ . In contrast, as demonstrated for the Sodankylä site in Finnish Lapland, the  
observed daily-mean  $T_2$  typically climbs several degrees above  $0^{\circ}\text{C}$  before all snow  
has vanished.

- 750 – The likely main reason for the fact that  $T_2$  in ECHAM5 stays close to  $0^{\circ}\text{C}$  in the snow  
melt season is that the surface energy budget (and hence the surface temperature  $T_s$ )  
is not computed separately for the snow-free and snow-covered parts of the grid cell.  
Thus, even if the diagnosed snow cover fraction is well below 1, the grid-mean  $T_s$  is  
not allowed to rise above  $0^{\circ}\text{C}$ . This acts to suppress the sensible heat flux (or even  
makes it negative), so  $T_2$  cannot rise much above  $0^{\circ}\text{C}$  either, and leaves too large  
a fraction of the grid-mean surface net radiation to be consumed in melting snow.
- 755 – There is another factor related to the treatment of surface energy budget, which also  
likely contributes to the too early snow-off: ECHAM5 does not include a canopy layer.  
Thus, in particular, the shielding of snow on ground by the overlying canopy is not  
accounted for, which leaves too much solar radiation available for melting snow. This  
may explain why the early bias of snow-off in ECHAM5 in western Russia is especially  
760 pronounced when compared with snow course measurements made in forests.

Overall, the present study highlights the fact that snow-off timing in an atmospheric GCM  
depends on the simulation of a number of processes: large-scale circulation and tempera-  
765 ture (which mainly determine the snowfall during winter), computation of snow properties on  
ground, treatment of surface albedo, and in general, the surface energy budget (which plays  
a key role for snow melt). In such a situation, as often in climate modeling, compensating  
errors are likely, so that improving any single process in the model may either improve or  
deteriorate the agreement with observations. An example of this is that for ECHAM5, the  
general tendency towards too early snow-off becomes clearer when biases in atmospheric  
770 circulation and temperature are corrected by nudging. This exposes more clearly the prob-  
lems related to the treatment of surface energy budget, especially in the presence of partial  
snow cover and forests. Beyond that, an obvious area for further development would be  
the snow scheme itself, which is rather simplistic in ECHAM5. Only the SWE and snow

temperature are computed, with no consideration of snow density and snow grain size. Furthermore, the temperature dependent snow albedo scheme in ECHAM5 is very simple and, as demonstrated in this and previous work, to some extent unrealistic.

Finally, according to our preliminary tests, snow melt also occurs at too low (grid-mean) temperatures in the Max Planck Institute's newest atmospheric GCM, ECHAM6 (Stevens et al., 2013). Like ECHAM5, ECHAM6 does not define separately the surface temperature for the snow-free and snow-covered parts of a grid cell. It is an intriguing question to which extent this issue pertains to other global and regional climate models.

## Appendix A: Determination of snow-off dates based on Russian snow course data

In the Russian snow course data (Bulygina et al., 2011a), SWE measurements are typically provided at 10 day intervals in winter and 5 day intervals in spring (starting from March or April). A major issue in defining the snow-off date based on these data is, however, that in the absence of snow, SWE measurements are generally not reported. Thus one cannot always be sure whether missing data indicates that there is no snow left to be measured, or that the measurement was not performed for some other reason. To define the snowmelt date, we adopted the following procedure.

1. The observation date with maximum SWE ( $d_{\max}$ ) for the winter was located.
2. The part of the SWE timeseries after  $d_{\max}$  was studied, and cases were sought in which a valid measurement of SWE was followed by missing data, with the corresponding dates denoted by  $d_{\text{miss}-1}$  and  $d_{\text{miss}}$ .
3. In such cases, it was assessed whether the missing data could plausibly indicate the absence of snow. For this end, we evaluated the statistics of SWE changes between two observation times (either 5 or 10 days apart from each other) within one month of the date in question, considering all years for which the station reported data. If the change in SWE from  $d_{\text{miss}-1}$  to  $d_{\text{miss}}$  required for all snow to melt by the time  $d_{\text{miss}}$

(i.e.,  $\Delta\text{SWE}_{\text{required}} = -\text{SWE}_{\text{miss}-1}$ ) was within two standard deviations ( $\sigma_{\Delta\text{SWE}}$ ) of the mean value ( $\overline{\Delta\text{SWE}}$ ) of SWE changes for the time of the year, that is,

$$\Delta\text{SWE}_{\text{required}} \geq \overline{\Delta\text{SWE}} - 2\sigma_{\Delta\text{SWE}}, \quad (\text{A1})$$

it was assumed that the missing SWE value at day  $d_{\text{miss}}$  indicates the absence of snow ( $\text{SWE}_{\text{miss}} = 0$ ).

4. If the missing value was deemed to be zero, all subsequent missing values were also interpreted as zero, until (possibly) a positive SWE value was found.
5. After the SWE time series was corrected as outlined above, the snow-off date was determined. Data for three observation days were used: the first observation day ( $d_{\text{zero}}$ ) with corrected  $\text{SWE} = 0$  after the winter's SWE maximum ( $d_{\text{max}}$ ), and the two observation days preceding it with  $\text{SWE} > 0$  (denoted as  $d_{m2}$  and  $d_{m1}$ , with SWEs of  $\text{SWE}_{m2}$  and  $\text{SWE}_{m1}$ , respectively). If linear extrapolation based on the values  $\text{SWE}_{m2}$  and  $\text{SWE}_{m1}$  suggested all snow to have melted before  $d_{\text{zero}}$ , the snow-off date was computed as

$$d_{\text{snow-off}} = d_{m1} + (d_{m1} - d_{m2}) \frac{\text{SWE}_{m1}}{\text{SWE}_{m2} - \text{SWE}_{m1}}, \quad (\text{A2})$$

otherwise, it was assumed that  $d_{\text{snow-off}} = d_{\text{zero}}$ .

6. Finally, if the SWE reached values higher than  $20 \text{ kg m}^{-2}$  after the determined snow-off date, the case was considered suspicious; thus this winter's data for this snow course were ignored in further analysis. Cases in which the above algorithm failed to find a snow-off date were likewise ignored in the subsequent analysis.

Clearly, the above algorithm involves some arbitrary choices (especially the criterion of 2 standard deviations in Eq. (A1) and the limit of  $20 \text{ kg m}^{-2}$  in step (6) of the algorithm). However, a number of sensitivity tests were conducted regarding the choice of these parameters, and it was found that the statistics of model vs. observation differences were

largely insensitive to them. For example, changing the criterion of 2 standard deviations in Eq. (A1) to either 1 or 3 standard deviations changed the average model vs. observation difference in snow-off dates by less than 1 day.

Lastly but importantly, to compare ECHAM5's snow-off dates with the snow course data as consistently as possible, the simulated SWE time series were first subsampled according to the availability of the snow course data (i.e., including only the days with measurements), and the snow-off dates for ECHAM5 were then determined according to the algorithm outlined above. For comparison with satellite data, however, the simulated snow-off dates were derived from the complete time series of daily-mean SWE.

*Acknowledgements.* This research was supported by the Academy of Finland (project numbers 116109, 140915 and 254195). The Russian Hydrometeorological Centre and the Climatic Research Unit, University of East Anglia, respectively, are acknowledged for making available the snow course data and the 2 m temperature data used in this study. Sebastian Rast (Max Planck Institute for Meteorology, Hamburg, Germany) is thanked for producing the ERA-Interim files for nudged ECHAM5 runs. Jaakko Ikonen (FMI) is thanked for help with the GlobCover data. Finally, thanks are due to Richard Essery and an anonymous reviewer for their helpful comments on the manuscript.

## References

- AMIP Project Office: AMIP II Guidelines. AMIP Newsletter, 8, available at: <http://www-pcmdi.llnl.gov/projects/amip/NEWS/amipnl8.php> (last access: 6 November 2014), 1996.
- Arino, O., Ramos Perez, J. J., Kalogirou, V., Bontemps, S., Defourny, P., and Van Bogaert, E.: Global land cover map for 2009 (GlobCover 2009), European Space Agency (ESA) and Université Catholique de Louvain (UCL), doi:10.1594/PANGAEA.787668, 2012.
- Armstrong, R. L., Knowles, K. W., Brodzik, M. J., and Hardman, M. A.: DMSP SSM/I Pathfinder Daily EASE-Grid Brightness Temperatures, Jan 1987–Jul 2008, National Snow and Ice Data Center, Boulder, Colorado, USA, digital media, 1994.
- Bontemps, S., Defourny, P., Van Bogaert, E., Arino, O., Kalogirou, V., and Ramos Perez, J. J.: GLOBCOVER 2009 Products description and validation report. Université Catholique de Louvain (UCL) and European Space Agency (ESA), Vers. 2.2,

- 53 pp., [http://epic.awi.de/31014/16/GLOBCOVER2009\\_Validation\\_Report\\_2-2.pdf](http://epic.awi.de/31014/16/GLOBCOVER2009_Validation_Report_2-2.pdf) (last access: 6 November 2014), 2011.
- 855 Brohan, P., Kennedy, J. J., Harris, I., Tett, S. F. B., and Jones, P. D.: Uncertainty estimates in regional and global observed temperature changes: a new data set from 1850, *J. Geophys. Res.*, 111, D12106, doi:10.1029/2005JD006548, 2006.
- Brown, R. D.: Northern Hemisphere snow cover variability and change, 1915–97, *J. Climate*, 13, 2339–2355, 2000.
- 860 Brown, R. D. and Robinson, D. A.: Northern Hemisphere spring snow cover variability and change over 1922–2010 including an assessment of uncertainty, *The Cryosphere*, 5, 219–229, doi:10.5194/tc-5-219-2011, 2011.
- Brutel-Vuilmet, C., Ménégoz, M., and Krinner, G.: An analysis of present and future seasonal Northern Hemisphere land snow cover simulated by CMIP5 coupled climate models, *The Cryosphere*, 7, 67–80, doi:10.5194/tc-7-67-2013, 2013.
- 865 Bulygina, O. N., Razuvaev, V. N., and Aleksandrova, T. M.: Description of data set “Routine snow surveys”, available at: <http://meteo.ru/english/climate/snow1.php> (last access: 6 November 2014), 2011a.
- Bulygina, O. N., Groisman, P. Ya., Razuvaev, V. N., and Korshunova, N. N.: Changes in snow cover characteristics over Northern Eurasia since 1966, *Environ. Res. Lett.*, 6, 045204, doi:10.1088/1748-9326/6/4/045204, 2011b.
- 870 Cohen, J.: Snow cover and climate, *Weather*, 49, 150–156, 1994.
- Dee, D. P., Uppala, S. M., Simmons, A. J., Berrisford, P., Poli, P., Kobayashi, S., Andrae, U., Balmaseda, M. A., Balsamo, G., Bauer, P., Bechtold, P., Beljaars, A. C. M., van de Berg, L., Bidlot, J., Bormann, N., Delsol, C., Dragani, R., Fuentes, M., Geer, A. J., Haimberger, L., Healy, S. B., Hersbach, H., Hólm, E. V., Isaksen, I., Kållberg, P., Köhler, M., Matricardi, M., McNally, A. P., Monge-Sanz, B. M., Morcrette, J.-J., Park, B.-K., Peubey, C., de Rosnay, P., Tavolato, C., Thépaut, J.-N. and Vitart, F.: The ERA-Interim reanalysis: configuration and performance of the data assimilation system, *Q. J. Roy. Meteor. Soc.*, 137, 553–597, 2011.
- 875 Derksen, C. and Brown, R.: Spring snow cover extent reductions in the 2008–2012 period exceeding climate model projections. *Geophys. Res. Lett.*, 39, L19504, doi:10.1029/2012GL053387, 2012.
- 880 Dickinson, R. E., Henderson-Sellers, A., and Kennedy, P. J.: Biosphere-atmosphere Transfer Scheme (BATS) Version 1e as Coupled to the NCAR Community Climate Model, NCAR Technical Note NCAR/TN-387+STR, doi:10.5065/D67W6959, 1993.

- 885 Essery, R., Rutter, N., Pomeroy, J., Baxter, R., Stähli, M., Gustafsson, D., Barr, A., Bartlett, P., and  
Elder, K.: SNOWMIP2: An evaluation of forest snow process simulations, *Bull. Amer. Meteor.  
Soc.*, 90, 1120–1135, doi:10.1175/2009BAMS2629.1, 2009.
- Fletcher, C. G., Zhao, H., Kushner, P. J., and Fernandes, R.: Using models and satellite obser-  
vations to evaluate the strength of snow albedo feedback, *J. Geophys. Res.*, 117, D11117,  
890 doi:10.1029/2012JD017724, 2012.
- Foster, J., Liston, G., Koster, R., Essery, R., Behr, H., Dumenil, L., Verseghy, D., Thompson, S.,  
Pollard, D., and Cohen, J.: Snow cover and snow mass intercomparisons of general circulation  
models and remotely sensed datasets, *J. Climate*, 9, 409–426, 1996.
- Frei, A. and Robinson, D. A.: Evaluation of snow extent and its variability in the Atmospheric Model  
895 Intercomparison Project, *J. Geophys. Res.*, 103, 8859–8871, 1998.
- Frei, A., Miller, J., and Robinson, D. A.: Improved simulations of snow extent in the second phase  
of the Atmospheric Model Intercomparison Project (AMIP-2), *J. Geophys. Res.*, 108, 4369,  
doi:10.1029/2002JD003030, 2003.
- Frei, A., Brown, R., Miller, J. A., and Robinson, D. A.: Snow mass over North America: observa-  
900 tions and results from the second phase of the Atmospheric Model Intercomparison Project, *J.  
Hydrometeorol.*, 6, 681–695, 2005.
- Gildea, M. P. and Moore, B.: FAOSOL – A global soil archive, Complex systems research center, Uni-  
versity of New Hampshire, Durham, New Hampshire (unpublished data tape and documentation),  
1985.
- 905 Groisman, P. Y., Karl, T. R., and Knight, R. W.: Changes of snow cover, temperature and radiative  
heat balance over the Northern Hemisphere, *J. Climate*, 7, 1633–1656, 1994.
- Hall, A. and Qu, X.: Using the current seasonal cycle to constrain snow albedo feedback in future  
climate change, *Geophys. Res. Lett.*, 33, L03502, doi:10.1029/2005GL025127, 2006.
- Heino, R. and Kitaev, L.: INTAS project (2002–2005): snow cover changes over  
910 Northern Eurasia during the last century: circulation consideration and hydro-  
logical consequences (SCCONE), *BALTEX Newsletter*, 5, 8–9, available at:  
[www.baltex-research.eu/publications/Newsletter/Newsletter5.pdf](http://www.baltex-research.eu/publications/Newsletter/Newsletter5.pdf) (last access: 6 Novem-  
ber 2014), 2003.
- Henderson-Sellers, A., Wilson, M. F., Thomas, G., and Dickinson, R. E.:  
915 Current global land-surface data sets for use in climate-related studies,  
NCAR Tech. Note NCAR/TN-272+STR, doi:10.5065/D6FQ9TK5, available at:

<http://opensky.library.ucar.edu/collections/TECH-NOTE-000-000-000-525> (last access: 6 November 2014), 1986.

920 Hurrell, J. W., Holland, M. M., Gent, P. R., Ghan, S., Kay, J. E., Kushner, P. J., Lamarque, J.-F., Large, W. G., Lawrence, D., Lindsay, K., Lipscomb, W. H., Long, M. C., Mahowald, N., Marsh, D. R., Neale, R. B., Rasch, P., Vavrus, S., Vertenstein, M., Bader, D., Collins, W. D., Hack, J. J., Kiehl, J., and Marshall, S.: The Community Earth System Model: a framework for collaborative research, *Bull. Amer. Meteor. Soc.*, 94, 1339–1360, doi:10.1175/BAMS-D-12-00121.1, 2013.

925 Kendon, E. J., Rowell, D. P, and Jones, R. G.: Mechanisms and reliability of future projected changes in daily precipitation, *Clim. Dynam.*, 35, 489–509, doi:10.1007/s00382-009-0639-z, 2010.

Kitae, L., Kislov, A., Krenke, A., Razuvaev, V., Martuganov, R., and Konstantinov, I.: The snow cover characteristics of northern Eurasia and their relationship to climatic parameters, *Boreal Environ. Res.*, 7, 437–445, 2002.

930 Knowles, K., Njoku, E., Armstrong, R., and Brodzik, M. J.: Nimbus-7 SMMR Pathfinder Daily EASE-Grid Brightness Temperatures, National Snow and Ice Data Center, Boulder, CO, USA, digital media and CD-ROM, 2002.

Liston, G. E.: Local advection of momentum, heat, and moisture during the melt of patchy snow covers, *J. Appl. Meteorol.*, 34, 1705–1715, 1995.

935 Liston, G. E.: Representing subgrid snow cover heterogeneities in regional and global models, *J. Climate*, 17, 1381–1397, 2004.

Lundquist, J. D., Dickerson-Lange, S. E., Lutz, J. A., and Cristea, N. C.: Lower forest density enhances snow retention in regions with warmer winters: A global framework developed from plot-scale observations and modeling, *Water. Resour. Res.*, 49, 6356–6370, doi:10.1002/wrcr.20504, 940 2013.

Metsämäki, S., Pulliainen, J., Salminen, M., Luojus, K., Wiesmann, A., Solberg, R., Böttcher, K., Hiltunen, M., and Ripper, E.: Introduction to GlobSnow Snow Extent products with considerations for accuracy assessment, *Remote Sens. Environ.*, 156, 96–108, doi:10.1016/j.rse.2014.09.018, 2015.

945 Mialon, A., Coret, L., Kerr, Y. H., Sécherre, and Wigneron, J.-P.: Flagging the topographic impact on the SMOS signal, *IEEE T. Geosci. Remote*, 46, 689–694, 2008.

Mölders N., Luijting, H., and Sassen, K.: Use of atmospheric radiation measurement program data from Barrow, Alaska, for evaluation and development of snow-albedo parameterizations, *Meteorol. Atmos. Phys.*, 99, 199–219, 2008.

- 950 Oleson, K. W., Lawrence, D. M., Bonan, G. B., Flanner, M. G., Kluzek, E., Lawrence, P. J., Levis, S.,  
Swenson, S. C., Thornton, P. E., Dai, A., Decker, M., Dickinson R., Feddema, J., Heald, C. L.,  
Hoffman, F., Lamarque, J.-F., Mahowald, N., Niu, G.-Y., Qian, T., Randerson, J., Running S.,  
Sakaguchi, K., Slater, A., Stöckli, R, Wang, A., Yang, Z.-L., Zeng, Xi., and Zeng, Xu.: Tech-  
955 nical Description of version 4.0 of the Community Land Model (CLM), NCAR Technical Note  
NCAR/TN-478+STR, National Center for Atmospheric Research, Boulder, CO, 257 pp., available  
at: [http://www.cesm.ucar.edu/models/cesm1.0/clm/CLM4\\_Tech\\_Note.pdf](http://www.cesm.ucar.edu/models/cesm1.0/clm/CLM4_Tech_Note.pdf), (last access: 6 Novem-  
ber 2014), 2010.
- Pedersen, C. A. and Winther, J.-G.: Intercomparison and validation of snow albedo parameterization  
schemes in climate models, *Clim. Dynam.*, 25, 351–362, 2005.
- 960 Pulvirenti, L., Pierdicca, N., and Marzano, S.: Topographic effects on the surface emissivity of  
a mountainous area observed by a spaceborne microwave radiometer, *Sensors*, 8, 1459–1474,  
2008.
- Qu, X. and Hall, A., What controls the strength of snow-albedo feedback?, *J. Climate*, 20, 3971–  
3981, 2007.
- 965 Qu, X. and Hall, A., On the persistent spread in snow-albedo feedback, *Clim. Dynam.*, 42, 69–81,  
doi:10.1007/s00382-013-1774-0, 2014.
- Räisänen, J.: Warmer climate: less or more snow?, *Clim. Dynam.*, 30, 307–319, 2008.
- Riihelä, A., Manninen, T., Laine, V., Andersson, K., and Kaspar, F.: CLARA-SAL: a global  
28 yr timeseries of Earth's black-sky surface albedo, *Atmos. Chem. Phys.*, 13, 3743–3762,  
970 doi:10.5194/acp-13-3743-2013, 2013.
- Roeckner, E., Bäuml, G., Bonaventura, L., Brokopf, R., Esch, M., Giorgetta, M., Hage-  
mann, S., Kirchner, I., Kornblueh, L., Manzini, E., Rhodin, A., Schlese, U., Schulzweida, U.,  
and Tompkins, A.: The atmospheric general circulation model ECHAM5, Part I, Model  
description, Max Planck Institute for Meteorology Rep. 349, 127 pp., available at:  
975 [www.mpimet.mpg.de/fileadmin/publikationen/Reports/max\\_scirep\\_349.pdf](http://www.mpimet.mpg.de/fileadmin/publikationen/Reports/max_scirep_349.pdf) (last access:  
6 November 2014), 2003.
- Roeckner, E., Brokopf, R., Esch, M., Giorgetta, M., Hagemann, S., Kornblueh, L., Manzini, E.,  
Schlese, U., and Schulzweida, U.: Sensitivity of simulated climate to horizontal and vertical reso-  
lution in the ECHAM5 atmosphere model, *J. Climate*, 19, 3771–3791, 2006.
- 980 Roesch, A.: Evaluation of surface albedo and snow cover in AR4 coupled climate models, *J. Geo-  
phys. Res.*, 111, D15111, doi:10.1029/2005JD006473, 2006.

- Roesch, A. and Roeckner, E.: Assessment of snow cover and surface albedo in the ECHAM5 general circulation model, *J. Climate*, 19, 3828–3843, 2006.
- Roesch, A., Wild, M., Gilgen, H., and Ohmura, A.: A new snow cover fraction parametrization for the  
985 ECHAM4 GCM, *Clim. Dynam.*, 17, 933–946, 2001.
- Rowell, D. P. and Jones, R. G.: Causes and uncertainty of future summer drying over Europe, *Clim. Dynam.*, 27, 281–299, 2006.
- Stevens, B., Giorgetta, M., Esch, M., Mauritsen, T., Crueger, T., Rast, S., Salzmann, M., Schmidt, H.,  
990 Bader, J., Block, K., Brokopf, R., Fast, I., Kinne, S., Kornblueh, L., Lohmann, U., Pincus, R., Reichler, T., and Roeckner, E.: Atmospheric component of the MPI-M Earth System Model: ECHAM6, *J. Adv. Model. Earth Syst.*, 5, 146–172, doi:10.1002/jame.20015, 2013.
- Strasser, U., Warscher, M., and Liston, G. E.: Modeling snow-canopy processes on an idealized mountain, *J. Hydrometeorol.*, 12, 663–677, 2011.
- Takala, M., Pulliainen, J., Metsämäki, S., and Koskinen, J.: Detection of snow melt using spaceborne  
995 microwave radiometer data in Eurasia from 1979 to 2007, *IEEE T. Geosci. Remote*, 47, 2996–3007, 2009.
- Tanré, D., Geleyn, J. F., and Slingo, J. M.: First results of the introduction of an advanced aerosol-radiation interaction in the ECMWF low resolution global model, in: *Aerosols and Their Climatic Effects*, A. Deepak Publishing, Hampton, Virginia, USA, 133–177, 1984.
- 1000 Versegny, D. L.: The Canadian Land Surface Scheme (CLASS): Its history and future, *Atmos. Ocean*, 38, 1–13, doi:10.1080/07055900.2000.9649637, 2000.
- von Salzen, K., Scinocca, J. F., McFarlane, N. A., Li, J., Cole, J. N. S., Plummer, D., Versegny, D., Reader, M. C., Ma X., Lazare, M., and Solheim, L.: The Canadian Fourth Generation Atmospheric Global Climate Model (CanAM4), Part I: Representation of physical processes, *Atmos. Ocean*, 51,  
1005 104–125, doi:10.1080/07055900.2012.755610, 2013.
- Wetherald, R. T. and Manabe, S.: The mechanisms of summer dryness induced by greenhouse warming, *J. Climate*, 8, 3096–3108, 1995.
- Yamazaki, T.: The influence of forests on atmospheric heating during the snowmelt season, *J. Appl. Meteorol.*, 34, 511–519, 1995.
- 1010 Zhao, H. and Fernandes, R.: Daily snow cover estimation from Advanced Very High Resolution Radiometer Polar Pathfinder data over Northern Hemisphere land surfaces during 1982–2004, *J. Geophys. Res.*, 114, D05113, doi:10.1029/2008JD011272, 2009.

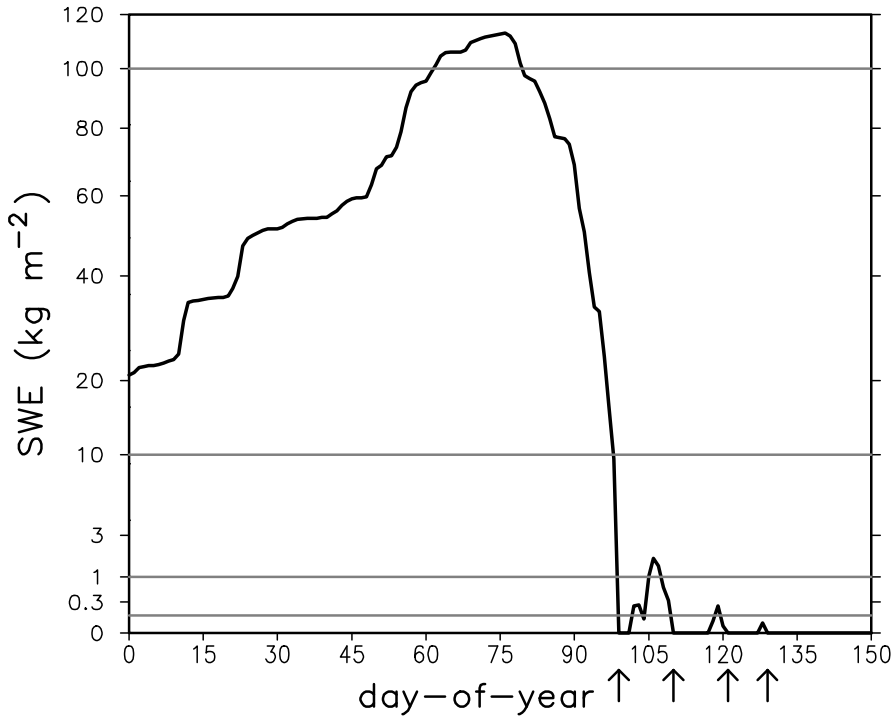


**Figure 1.** Time series of snow water equivalent ( $\text{kg m}^{-2}$ ) in days 0–150 of year 1988 for a grid cell in western Russia ( $60.6^\circ \text{N}$ ,  $39.4^\circ \text{E}$ ) for one of the ECHAM5 runs included in the REF experiment (SWE plotted in a square root scale for a better viewing of small values). The grey horizontal lines correspond to SWE values of  $100 \text{ kg m}^{-2}$ ,  $10 \text{ kg m}^{-2}$ ,  $1 \text{ kg m}^{-2}$ , and  $0.1 \text{ kg m}^{-2}$ . The four arrows at days 99 (8 April), 110 (19 April), 121 (30 April) and 129 (8 May) indicate possible snow-off days (first day with  $\text{SWE} = 0$  after a period with  $\text{SWE} > 0$ ). The first snow-off day is employed in this paper for comparison with observational data.

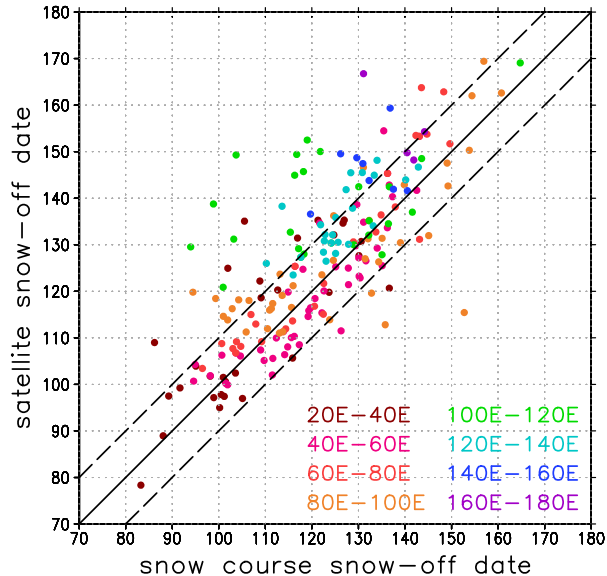


**Figure 2.** The relationship between time-mean snow-off dates based on the snow course data and the satellite retrievals. The satellite snow-off dates were averaged to the T63 horizontal resolution and screened according to the availability of snow course data. Only those grid cells for which the snow-off date in the snow course data could be determined for at least five years during 1979–2006 are included. The data points are colour-coded according to longitude. The solid diagonal line indicates equal snow-off dates for the two datasets, while the dashed diagonals correspond to a difference of  $\pm 10$  days.

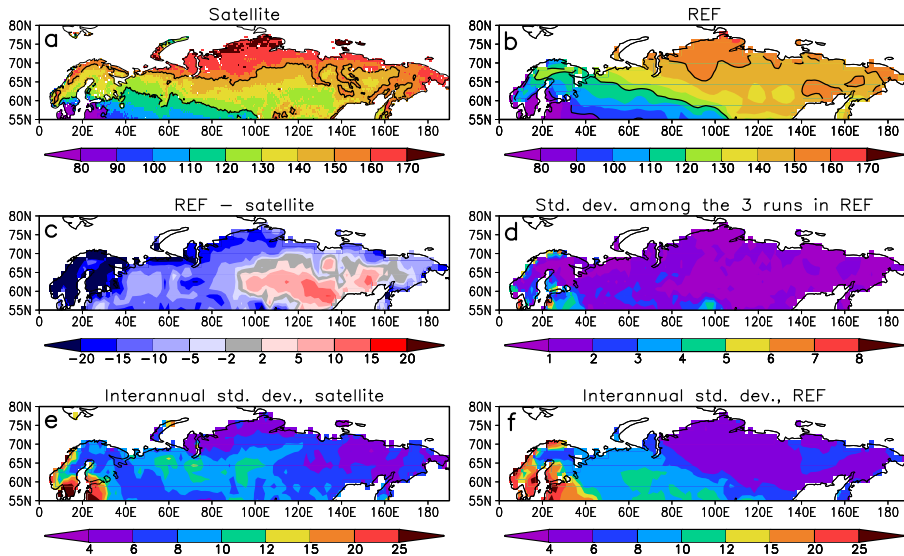


**Figure 3.** Mean snow-off date in years 1979–2006 based on (a) the satellite retrievals and (b) the REF experiment. Unit: day of year (Julian day). Snow-off dates of 90, 120 and 150 corresponding approximately to the beginning of April, May and June are indicated with black lines. (c) The difference in the average snow-off date between the REF experiment and the satellite retrievals. For computing the difference, the satellite snow-off dates were averaged to the model grid. (d) The standard deviation ( $\sigma_{n-1}$ ) in 28 year mean snow-off date among the  $n = 3$  differently initialized runs included in the REF experiment. (e) The standard deviation of yearly snow-off dates in the satellite retrievals (for snow-off dates averaged to the model grid), and (f) in the REF experiment (computed first separately for the three runs in REF and then averaged).

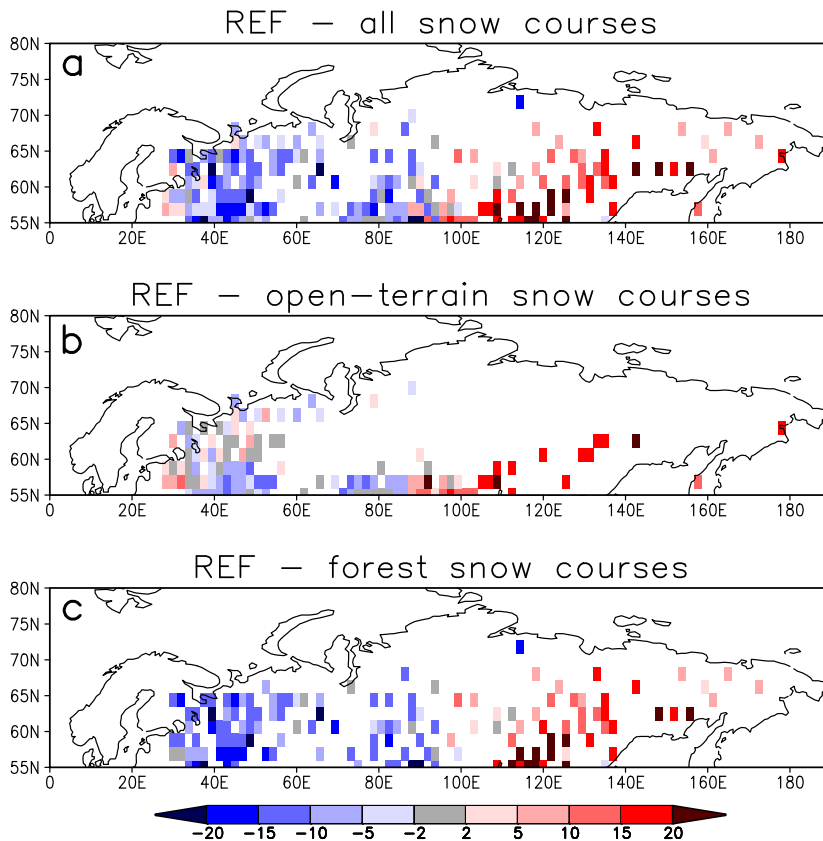


**Figure 4.** The difference in the average snow-off date for years 1979–2006 between the REF experiment and Russian snow course data for (a) all snow courses, (b) open-terrain snow courses, and (c) forest snow courses. Only those grid cells with snow-off data for at least five years are included.

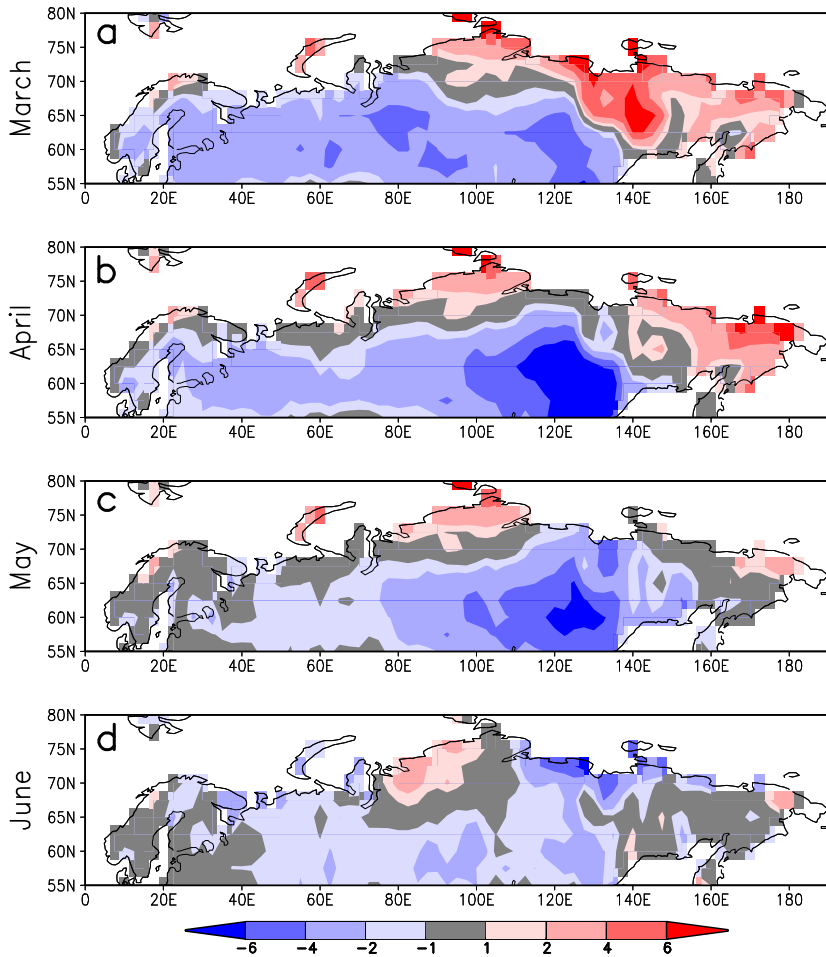


**Figure 5.** Differences in 2 m air temperature [K] for years 1979–2006 between the REF experiment and the CRUTEM3 dataset for the months of March, April, May and June.

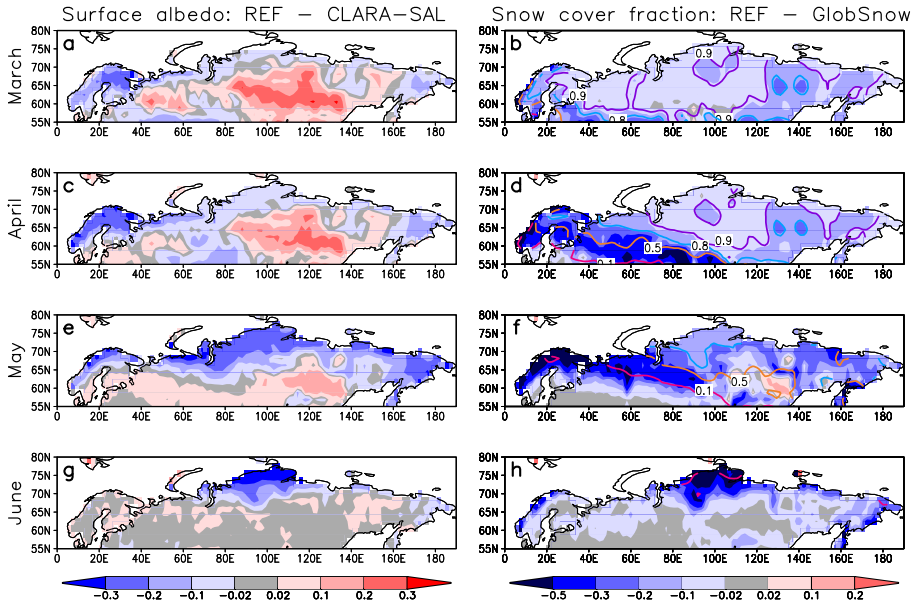


**Figure 6.** (a,c,e,g): Differences in surface albedo for years 1982–2006 between the REF experiment and the CLARA-SAL dataset for the months of March, April, May, and June. (b,d,f,h): Corresponding differences in snow cover fraction for years 1997–2006 (excluding 2002) between the REF experiment and the GlobSnow dataset. The coloured contours (magenta = 0.1; orange = 0.5; blue = 0.8; and violet = 0.9) indicate the snow cover fraction in REF.

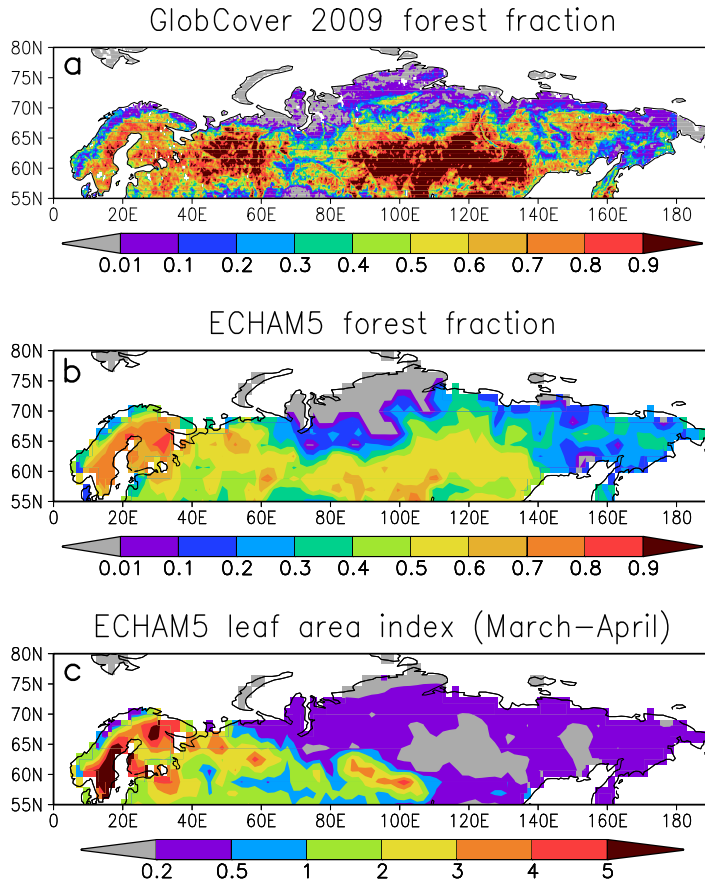


**Figure 7.** (a) Forest fraction in the GlobCover 2009 land cover map (computed as the sum of land cover classes 40, 50, 60, 70, 90 and 100). (b) Forest fraction assumed in the ECHAM5 simulations. (c) Leaf area index assumed in the ECHAM5 simulations, averaged over March and April.

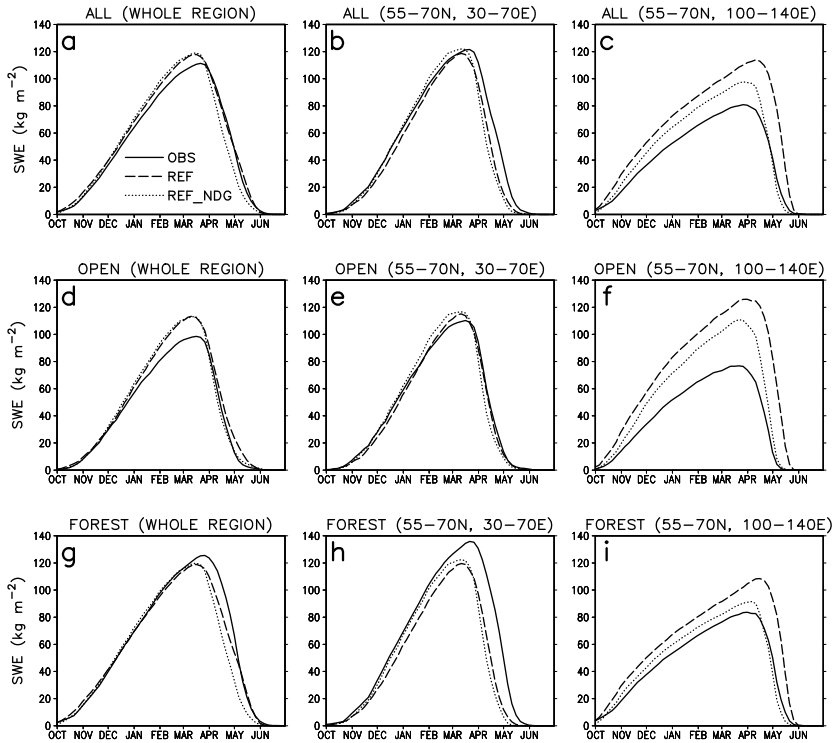


**Figure 8.** Mean annual cycle of SWE according to the snow course measurements (solid line), in the REF experiment (dashed line) and in the REF\_NDG experiment (dotted line) for **(a)** all snow courses for the whole Northern Eurasian domain, **(b)** for Western Russia (55–70° N, 30–70° E) and **(c)** for Eastern Siberia (55–70° N, 100–140° E). **(d–f)**: as **(a–c)** but including only open-terrain snow courses. **(g–i)**: as **(a–c)** but including only forest snow courses. Only those ECHAM5 grid cells with snow course data are included in the domain-mean values. For clarity, results for the ALB1, ALB2, ALB1\_NDG and ALB2\_NDG experiments are not shown. In general, albedo changes had little effect on SWE, except for the snow melt season.

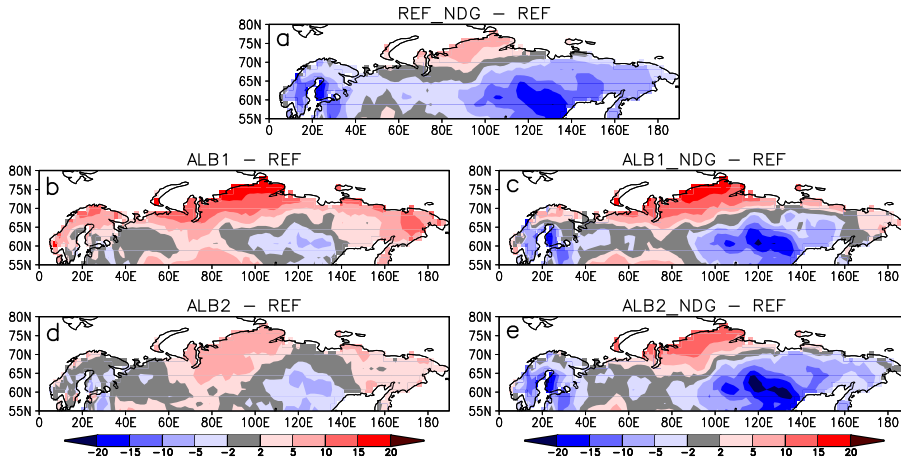


**Figure 9.** Differences in average snow-off date between the five sensitivity experiments (REF\_NDG, ALB1, ALB1\_NDG, ALB2 and ALB2\_NDG) and the REF experiment.

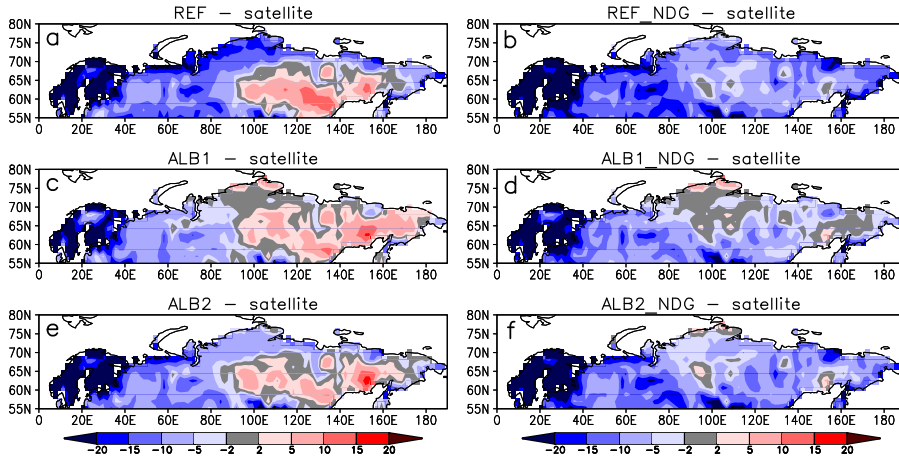


**Figure 10.** Differences in average snow-off date between the six ECHAM5 experiments and the satellite retrievals.

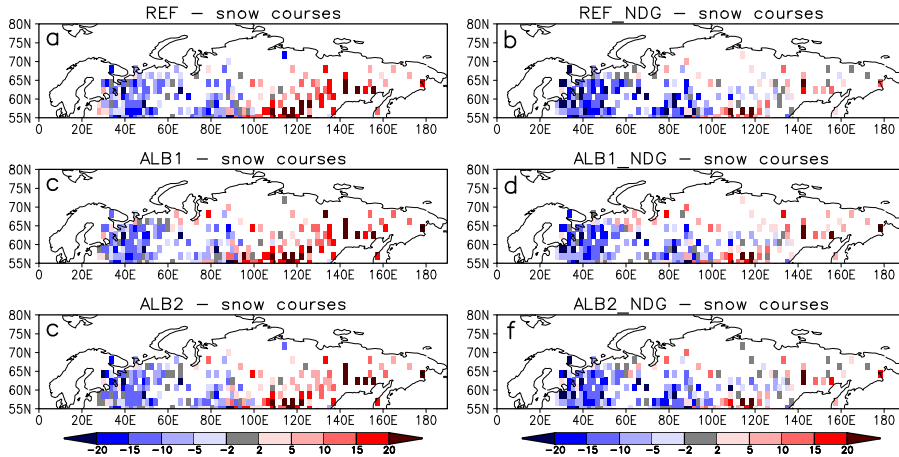


**Figure 11.** Differences in average snow-off date between the six ECHAM5 experiments and the Russian snow course data. Both open-terrain and forest snow courses are included in the comparison.

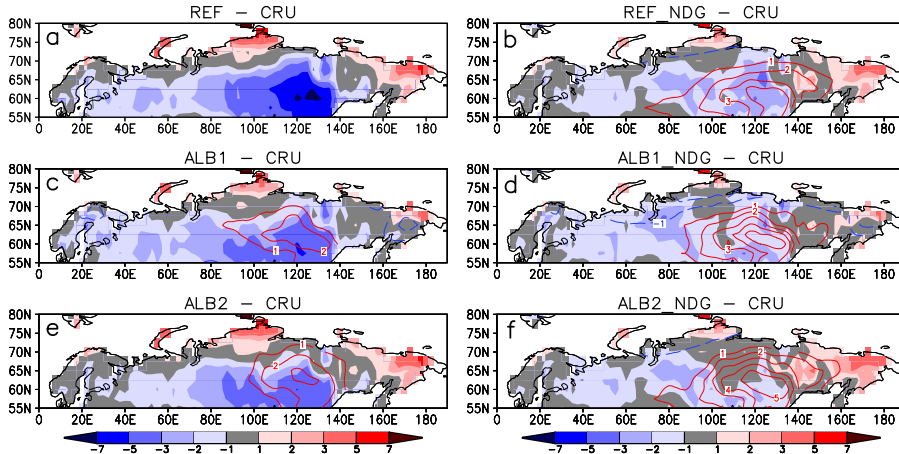


**Figure 12.** Differences in April–May mean 2 m air temperature between ECHAM5 and the CRUTEM3 dataset for the (a) REF, (b) REF\_NDG, (c) ALB1, (d) ALB1\_NDG, (e) ALB2 and (f) ALB2\_NDG experiments. The contours in (b–f) indicate the difference from the REF experiment (contour interval 1 K; zero contour omitted).

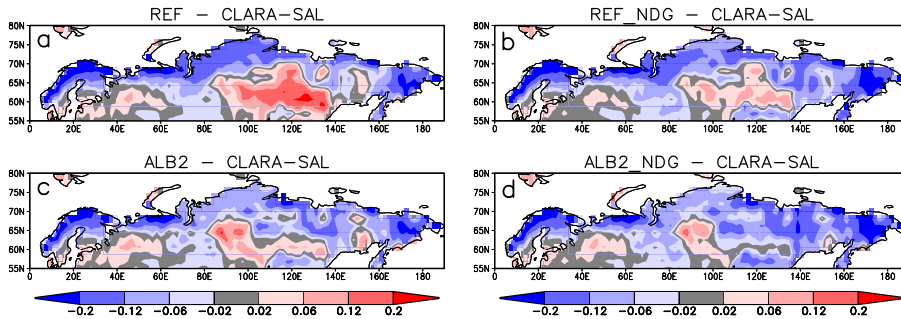


**Figure 13.** Differences in April–May mean albedo between ECHAM5 and the CLARA-SAL dataset for the (a) REF, (b) REF\_NDG, (c) ALB2 and (d) ALB2\_NDG experiments. In ALB1 and ALB1\_NDG (not shown) the albedo values are, by construction, identical to the CLARA-SAL data.

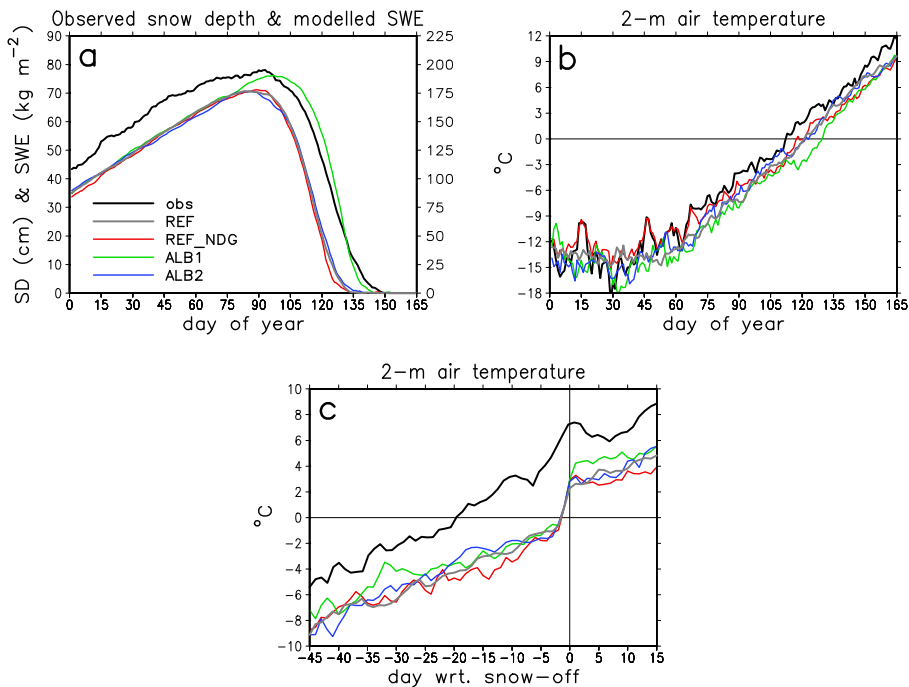


**Figure 14.** Comparison of ECHAM5 simulations with observations at Sodankylä (67.37° N, 26.63° E). **(a)** Mean seasonal cycle of observed snow depth (black line, scale on the left) and modelled SWE (four curves for different ECHAM5 experiments, scale on the right) in 1979–2006. **(b)** Mean seasonal cycle of 2 m air temperature. **(c)** Mean 2 m air temperature composited with respect to the snow-off date, “day 0” representing the first completely snow-free day. The ECHAM5 results are taken from the grid point nearest to the Sodankylä site (68.08° N, 26.25° E).